UNIVERSITY MICROFILMS, INC., ANN ARBOR, MICH.

L. C. Card no. Mic 59- 2109

DOOLITTLE II, Robert Frederick.

THE LATERAL STRUCTURE NEAR THE CORE OF LARGE AIR SHOWERS.

University of Michigan, Ph. D., 1959
Physics, general

Negative microfilm received from university.

THE LATERAL STRUCTURE NEAR THE CORE OF LARGE AIR SHOWERS

by

Robert F. Doolittle II

A dissertation submitted in partial fulfillment
of the requirements for the degree of
Doctor of Philosophy in the
University of Michigan
1958

Doctoral Committee:

Professor Wayne E. Hazen, Chairman
Assistant Professor Donald A. Gilbert
Assistant Professor William C. Meecham
Associate Professor Peter A. S. Smith
Professor Marcellus L. Wiedenbeck

ACKNOWLEDGMENTS

It is with great pleasure that I take this opportunity to express my sincere gratitude and appreciation to Professor Wayne E. Hazen, who not only suggested this problem, but who was always willing to devote many hours to helpful discussions and advice throughout its completion. His guidance and encouragement has, indeed, been very much appreciated.

I am indebted to Mr. Martin H. LaPointe and Mr. John F. Gaebler who contributed their services to many phases of the operation and maintenance of the equipment.

I also wish to thank Mr. Lo-I Yin who spent many tireless hours scanning film and helping in the reduction of the data.

This research was supported by a grant to the cosmic ray program of the University of Michigan from the joint program of the Atomic Energy Commission and the Office of Naval Research.

TABLE OF CONTENTS

	Page
ACKNOWLEDGMENTS	ii
LIST OF ILLUSTRATIONS	v
I. INTRODUCTION	1
1.1 Historical Background and Discovery of Large Air Showers	1
1.2 Recent Developments	4
1.3 The Purpose of the Present Experiment	5
II. THE SHOWER STRUCTURE PROBLEM	7
2.1 Cascade Theory	7
2.1.1 The Longitudinal Development	8
2.1.2 The Lateral Spread	10
2.2 Previous Experiments on the Lateral Spread	13
2.3 The General Problem Near the Shower Axis	22
2.4 Theoretical Considerations Near the Shower Axis	23
2.5 The Method and Location of the Present Experiment	24
III. EXPERIMENTAL APPARATUS	28
3.1 Introduction	28
3.2 The Multiwire Ionization Chambers	30
3.2.1 The Single Wire Ionization Chambers	32
3.3 The Argon Gas System	33
3.4 The Amplifiers	38
3.5 The Geiger Counters	41
3.6 The Coincidence Circuit	41
3.7 The Synchroscopes	41
3.8 The Camera	43
3.9 The Precision Pulser	43
3.10 The Film Reader	44
IV. THE EXPERIMENTAL METHOD	46
4.1 The Principles of Ionization Chamber Operation	46
4.2 Method of Calibration	48
4.2.1 Amplifier Calibration Procedures	52
4.2.2 The α-Particle Calibration	53

TABLE OF CONTENTS CONT'D

		Page
4.3	The Electron Attachment Problem.....	54
4.4	Experimental Errors.....	56
V.	METHOD OF ANALYSIS AND INTERPRETATION OF EXPERIMENTAL RESULTS.....	60
5.1	Ionization Chamber Theoretical Response Curves..	60
5.2	Systematic Deviations from the Response Curve and Fluctuations.....	63
5.3	The Selection of Individual Events for Analysis and Method of Presentation.....	6.
5.4	Individual Events and Their Interpretation.....	68
5.5	The Absolute Shower Rate.....	[illegible]
5.6	General Discussion of Results.....	94
5.7	Summary and Conclusions.....	95
APPENDIX A.....		98
APPENDIX B.....		103
BIBLIOGRAPHY.....		105

LIST OF ILLUSTRATIONS

Figure		Page
1	Plan View of Ionization Chamber Geometry.....	26
2	Block Diagram.....	29
3	Schematic Diagram of Gas System.....	34
4	Amplification Curve.....	39
5	Saturation Curve for MW Chambers.....	57
6	Saturation Curve for SW Chambers.....	57
7	Ionization Chamber Response Curves for s = 1.4, N = 10^5	61
8	Coordinate System in Observational Plane.....	62
9	Event #3493.....	66
10	Event #3310.....	67
11	Event #3951.....	70
12	Event #4006.....	71
13	Event #3635.....	72
14	Event #3765.....	74
15	Event #3334.....	75
16	Event #4109.....	77
17	Event #4089.....	79
18	Event #3148.....	80
19	Event #4085.....	82
20	Event #3076.....	83
21	Event #3567.....	85
22	Event #4127.....	86

LIST OF ILLUSTRATIONS CONT'D

Figure		Page
23	Event #3426.....	88
24	Event #3794.....	89
25	Triggering Probability Loci for $N = 5 \times 10^4$, $s = 1.3$.	92

CHAPTER I

INTRODUCTION

1.1 Historical Background and Discovery of Large Air Showers

The study of large air showers has been one of the most important tools used to obtain information about the primary cosmic rays, as well as their interactions with matter. It had been known since 1932 that the interactions of the primary cosmic rays with matter produced high energy secondary particles, and in the next few years many complex and puzzling events were recorded[1-3]. These experiments made use of cloud chambers and/or geiger counters, and indicated that ionizing particles were apparently multiplied when incident upon an absorber. It was also noted that ionizing particles were created, presumably, by the absorption of a neutral particle. These interactions were at first believed to be nuclear in origin. However, in 1933, it was shown[3] that the secondary ionizing particles were electrons and positrons. The problem remained essentially unsolved until 1935, when the process of pair production by high energy photons was suggested as possibly playing a role in the cascade process. Shortly thereafter, this hypothesis was experimentally confirmed, and the simultaneous development of quantum electrodynamics, which predicted that at high energies electrons lose their energy primarily by radiation, completed the picture.

The process, then, is one in which a high energy electron interacts with the Coulomb field of a nucleus and emits bremsstrahlung photons of somewhat lower energy. Each of these, in turn, is capable of materializing into an electron-positron pair, each of which may again emit radiation

and so on. In this manner a cascade shower develops longitudinally. This multiplication process continues until the original energy has been so subdivided that ionization rather than radiation becomes the predominant mode of energy loss for the electrons and they soon become absorbed. Beyond the point where the number of particles absorbed by ionization losses becomes larger than the number of particles produced by multiplication, the total number of particles decreases and thus a shower maximum may be defined. In the theory this corresponds to the so-called age parameter "s" being equal to unity. For "younger" showers $s < 1$, and for showers observed beyond their maximum $s > 1$.

The shower axis or core is defined as the direction of the primary initiating particle projected to the observational level. Were it not for Coulomb scattering of the electrons and the angular divergence of the secondaries, the particle density on the axis would, theoretically be infinite. The effect of the angular divergence of the secondaries can be shown to be negligible compared to Coulomb scattering, so that the lateral spread perpendicular to the shower axis is attributed almost entirely to multiple scattering.

Some of the quantities of interest in dealing with shower theory are defined as follows. The critical energy ϵ_0 is that energy which an electron must have in order that the probability of energy loss by ionization is equal to the probability of energy loss by radiation. Alternatively, it may be defined as that energy which an electron must have in order to be completely absorbed, by collision processes alone, in traversing an absorber of thickness equal to one radiation length. A radiation length

X_o is that thickness of material through which an electron must pass in order to have its energy reduced to $\frac{1}{e}$ of its original energy by radiation losses alone.

If now the constant E_s,[21] which has the dimensions of energy is introduced, one may define the characteristic scattering length as

$$r_1 = \frac{E_s}{\epsilon_o} X_o \quad .$$

This is a measure of the lateral spread, and if all distances are measured in units of r_1, then the lateral distribution is practically independent of the absorber.

In 1938, Auger, Maze, and Grivet-Meyer[4] and also Kolhörster, Matthes, and Weber[5] found cosmic ray events which caused coincidences between counters separated by as much as 10 meters in a horizontal plane. Further work[6], using a cloud chamber, showed these events to be electrons which were actually dispersed over distances of several hundred meters. These events were shown to be large cascade showers developing in air. They have been termed large, extensive, and giant air showers, or Auger showers. It is now known that these showers are not a particular type of cosmic ray phenomenon, but are the common sequence of interactions following the incidence of any high energy primary cosmic ray particle on the atmosphere. The only characteristic feature of the large air showers is the very high energy of the primary particle. This makes it possible for the shower to develop through many radiation lengths of the atmosphere and still have a sufficient density of secondaries to make possible its detection in a small volume at the observational level.

1.2 Recent Developments

It was originally believed that very high energy electrons or photons, incident on the upper atmosphere, were responsible for the phenomena. However, in the last ten years, it has been shown both theoretically and experimentally that there are practically no high energy photons or electrons in the primary cosmic radiation. Furthermore, it was later learned that the showers, once initiated, were not simple electron-photon cascades but had a more complex nature. It had been noticed that large air showers contained particles more penetrating than photons or electrons, and later it was shown that all large air showers contained penetrating particles and that all showers of penetrating particles were accompanied by large air showers[7,8]. Still more recently, another component was found to be associated with large air showers.[9,10,11] This component, called the N-component, was found to undergo strong nuclear interactions. It was subsequently determined that the penetrating particles were μ-mesons and the N-component was composed primarily of nucleons and charged π-mesons.

Since π-mesons and neutrons are unstable, they cannot have been part of the primary cosmic radiation, and hence the presence of the N-component indicates that one or more nuclear interactions must have taken place in the course of the shower's development. The question naturally arose then as to whether the soft component (electrons and photons) and the N-component had a common origin, or whether one was secondary to the other. When it was discovered[12] that a neutral π-meson was created along with charged π-mesons in nuclear interactions, and that the π^0 decayed very quickly into two photons, the hypothesis was made that the soft and

N-components had a common origin. In particular it was concluded from several cloud chamber experiments[13,14] that at least 80 per cent of all photons associated with nuclear events were created by means of a π^0-decay; and further, that all cascade showers showing the presence of an N-component were photon and not electron initiated.

On the basis of this evidence a cascade shower may be pictured as being initiated, along with the N-component cascade, in the primary interaction. The N-component, having a large cross section for interactions producing π^0-mesons, continuously contributes to the soft component as the shower develops. It has been shown[12,15] that usually there should be more than one π^0-meson created in each nuclear interaction. Then, since each π^0-meson decays into two photons, one would expect to find evidence of multiple core structures in most large air showers. Most experiments to date, however, have failed to show evidence of such structure other than showing a flatter distribution than that predicted by Moliere[16]. There have been a few experiments[17-20], nevertheless, which have indicated some "multiple peaked" events near the core, but the evidence is not conclusive since the observed phenomena may also be explained by the local creation of young cascades by the N-component. These and other recent experiments will be discussed in more detail in Section 2.2.

1.3 The Purpose of the Present Experiment

Since the lateral distribution of large air showers within a few meters of the core is not yet well known, the present experiment was designed to obtain additional, more definitive information in this region. A knowledge of the lateral distribution can in turn provide information about the origin of such showers.

The lateral electron distribution of a number of individual showers was examined and compared with the recent theory of Nishimura and Kameta,[34-36] which predicts the lateral distribution of electrons of all energies as a function of the shower age-s. Since the fluctuations in the effect of the N-component cascade are believed to be small, one may expect either events whose various cascade axes are so close together that the result is the same as for a single electronic cascade or events in which one electronic showers carries nearly all the energy at the observational level. In this way the structure of a single electronic cascade can be determined and compared with theory. If some showers show a more complex structure than indicated above, then it is expected that additional information on the N-component and the showers' origin may be obtained. A general discussion of the method used to accomplish this purpose is given in Section 2.5, and the experimental apparatus itself is described in detail in Chapter III.

It will also be possible in this experiment to calculate the absolute intensity, i.e. the frequency of occurrence of showers having a total number of electrons larger than N as a function of N, and to compare this with theory and with previous determinations. This will be discussed in Section 5.5.

CHAPTER II

THE SHOWER STRUCTURE PROBLEM

2.1 Cascade Theory

To describe completely the behavior of large air showers the following information would be necessary: the probability that, for an electron initiated shower, a given number of electrons of energy E would be observed in dE at a depth t in an absorber and at a distance r from, and making an angle θ with, the shower axis. A similar probability function would also be necessary for photons as well as the probabilities for observing the same quantities for photon initiated showers.

Now, the elementary processes involved in the development of a shower are well established by experiment and theory, but it is in appropriately combining these processes, to describe the actual behavior of the showers, that the problem becomes mathematically quite formidable.

It has therefore become customary immediately to make two simplications in treating air showers. The first simplification consists of subdividing the problem into two essentially independent problems, namely, the longitudinal development and the lateral spread. This treatment is justified if the path length of the particles projected upon the axis is approximately the same as their actual path length. This condition is satisfied for materials of low atomic number, such as air.

The second simplification consists of treating only the average behavior of the showers, as rigorously as possible, and then using a simplified model to treat fluctuations from the average.

The general results of the theory which pertain to the present experiment will now be presented. The detailed calculations and results may be found in Rossi and Greisen[21] and a more recent discussion in Rossi[22].

2.1.1 The Longitudinal Development

A knowledge of the average longitudinal development is necessary in order to relate the size of the showers observed to the energy and height of the initiating particle. For a large air shower, the total energy E_o of the primary is so high that at the observational level there is no significant difference between photon initiated and electron initiated showers. Then the only quantities of interest are the differential and integral spectra. The differential spectra are denoted by $\pi(E_o, E, t)$ and $\gamma(E_o, W, t)$, where πdE is the average number of electrons and γdW is the average number of photons of energy E or W in an interval dE or dW, respectively, at a depth t in the absorber, when the initiating particle or radiation has an energy E_o. The integral spectra are denoted by $\Pi(E_o, E, t)$ and $\Gamma(E_o, W, t)$, where Π and Γ are the total number of electrons or photons with energies greater than E or W, respectively.

To facilitate the calculation of these functions, it is customary, following Rossi and Greisen[21], to make one of two physical approximations. In "Approximation A", energy losses by collision and Compton effect are neglected. Thus, this is

an asymptotic solution for high energies where the dominant processes are radiation losses by electrons and pair production by photons. The longitudinal shower problem can be completely solved in this approximation and the results are valid for electron energies E, large compared to the critical energy ϵ_o, but small compared to the initiating energy E_o. In "Approximation B", energy loss by collision is included, but only by assuming a constant loss per electron per radiation length. The problem in this approximation has been only partially solved. Here, the results are valid for electrons whose energies are of the order of the critical energy or larger, but still small compared to the initiating energy. "Approximation B" also disregards all electrons whose energy becomes less than 5×10^6 ev as making no further contributions to the shower. This is justified since the range of electrons of this energy in air is much less than a radiation length. Greisen[23] has estimated that the average behavior for air showers, as calculated under "Approximation B", is accurate to about 10 per cent as far as the total number of electrons and the shape of the energy spectrum for $E > \epsilon_o$ are concerned.

When a shower is first initiated, i.e. when $s \cong 0$, the fluctuations from the average are largest since the particles do not interact independently of one another. As the shower develops the fluctuations decrease, reaching a minimum when the shower is at its maximum. This is because the number of electrons being lost by ionization is about equal to the number

being produced in the high energy core. The fluctuations from the average again increase as the shower develops beyond its maximum since the time required for the total energy to be dissipated depends on whether the shower had an early or late development. Additional sources of fluctuations are variations in the depth at which the first nuclear interaction occurs and statistical fluctuations in the types of secondaries produced and in their energy distribution.

2.1.2 The Lateral Spread

It has already been mentioned that the dominant mechanism responsible for the lateral spread is multiple scattering. This is the effect produced by many random small angle Coulomb scatterings.

Many authors[16,24-41] have published calculations on either the even moments of the distribution, i.e. r^n (where n is even) times the distribution function integrated over r, or the lateral distribution functions themselves. Although the treatment has been fairly successful for the high energy region, for energies less than 2 ϵ_o the solutions have been very approximate, especially for small distances from the core.

The quantities of interest would be the average radial distribution functions P_r (E, r, s) and Q_r (W, r, s), where $P_r dE$ is the relative number of electrons of energy E in dE at any angle with and at a distance r from the axis of a shower whose age is s, and $Q_r dW$ is the corresponding number of photons of

energy W in dW. By integrating P_r (E, r, s), say, over all energies one could then, in principle, find the radial distribution function f_r (0, r, s) for electrons of all energies.

The first complete theory of the lateral spread, in that an attempt was made to derive the radial and angular distributions for electrons of all energies at the shower maximum, was due to Moliere[16]. He took as his starting point the diffusion equations originally set up by Landau[25], and which have also been the basis of most subsequent theories. Moliere succeeded in deriving analytical equations for the distribution functions for high energy electrons under "Approximation A", i.e. for those whose energies are very much larger than the critical energy. He then proceeded to calculate the low energy contribution to the total distribution function by means of an approximation due to Arley[42] which is admittedly inexact. As Moliere himself pointed out there is an overestimate of the number of particles at energies near the critical energy and an underestimate of the number of low energy particles due to the Arley approximation. Since these effects are partially compensating there has been fair experimental agreement with the theory. A much-used analytical approximation to the Moliere distribution has been suggested by Bethe[51] and is the following:

$$xf(x) = 0.45\ (1 + 4x)\ e^{-4x^{2/3}} ,$$

where $x = \frac{r}{r_1}$, and the actual density Δ at x is given by $\Delta = \frac{Nf(x)}{r_1^2}$ where N is the total number of particles.

In the Moliere theory, as well as in other early theories, the age parameter s was a function only of the primary energy E_o and the depth t in the absorber. However, Nishimura and Kamata[34-36] have published a solution of the Landau equations for the total number of particles at any depth. Their theory correctly treats energy loss by ionization. As a consequence of their theory s is also a function of r, s increasing slowly as r decreases. Physically, this corresponds to the fact that the high energy particles near the axis reach their maximum earlier than the lower energy particles at greater distances from the axis. Nishimura and Kamata have presented graphs for the lateral distribution, based on numerical calculations, for s = 1 and s = 1.4. Greisen[23] has derived the following empirical formula for the Nishimura and Kamata distribution which fits well for s = 1 and s = 1.4 (and presumably for intermediate values as well):

$$xf(x) = C(s)\, x^{s-1}(x + 1)^{s-4.5}, \qquad (1)$$

where $C(s) = 0.445\, s^2\, (1.90-s)$.

The validity of this distribution has been well established by experiment for distances greater than a few meters from the core. For the present experiment it will be assumed that the above distribution is correct <u>within</u> a few meters of the axis

and proposed fits based on this distribution will be superimposed upon the experimental data.

2.2 Previous Experiments on the Lateral Spread

There have been, in general, four types of experiments designed to extract information on the lateral structure. First are the so-called decoherence curves, which are plots of n-fold geiger coincidence or biased ionization chamber coincidence rates versus their separation in a horizontal plane. These rates should be determined, at least in part, by the lateral distribution. However, since this method depends on other factors than the density distribution, it is not a very sensitive type of experiment.

Second, experiments have been performed using either geiger tubes or cloud chambers to obtain the integral density spectrum. In these experiments the number of events, in which the electron density at a given observational point is greater than some given density, is plotted against that density. Again, the density spectrum should yield some information about the density distribution.

The third method consists of observing directly, with a cloud chamber, the incident shower electrons and the electron pairs produced by the incident shower photons.

The fourth method, and the one which has been used in the present experiment, is to place a number of ionization chambers in a given geometrical array, and thus directly sample the electron density at a number of predetermined points in a horizontal plane.

In all four methods the quantity of interest is the density of particles at a given point. In this sense, the first method using geiger counters is indirect since the probability of observing a count is not a sharply varying function of density. In fact, the geiger counter data are integrals over ranges of densities. This, of course, is not true for ionization chamber and cloud chamber measurements.

The geiger counter data are analyzed by first obtaining a theoretical decoherence curve for an assumed lateral distribution. This is done by first integrating the probability of a coincidence for a given counter separation and given size shower over all possible locations of the shower axis in the observational plane, and then integrating over the shower integral number spectrum S (N), where $N \equiv \Pi (E_o, 0, t)$. The number spectrum is defined as the frequency of showers having a total number of electrons N in an interval dN and having an axis that crosses a unit area. To find S (N) a power law spectrum for primary electrons is usually assumed and then the results of longitudinal shower theory are applied to determine S (N) at the plane of observation. The resulting theoretical decoherence curve is then fit to the data by varying both the absolute rate of the primary spectrum and the exponent.

The second type of experiment is also rather insensitive for studying the lateral distribution since, again, the primary rate and spectrum must be assumed. However, these experiments do give the exponent in the number spectrum. This exponent is almost a constant but does vary slowly with N and with altitude.

Since the present experiment is primarily concerned with the lateral distribution, and since the first two methods mentioned above do not give definitive information about this distribution, the previous experiments employing these methods will not be discussed at length.

Most of the previous experiments concerning the lateral structure may be grouped into three categories depending on the distance from the core at which the lateral structure was investigated. First, following Greisen[23], medium distances may be defined as that region in which $0.03 < \frac{r}{r_1}, < 2.0$.

An interesting experiment in this category was performed at 3260 meters altitude by Cocconi, Tongiorgi, and Greisen[42] in which they used an unshielded counter in coincidence with four additional counters shielded by 9 cm of lead. It was hoped that the shielded counters would respond only to the high energy core and the unshielded counter would provide the discrimination necessary to eliminate local nuclear events occurring in the lead. They found that their "core selector" was, in fact, triggered almost entirely by showers whose cores struck within a few meters of the selector. To sample the electron density, they had groups of unshielded counters at varying distances from the core selector. They found that the density could be measured within a factor of two, as long as it was somewhere in the range between 2 and 500 particles per square meter. By comparing their average relative densities as a function of r with the theory of Nishimura and Kamata, excellent agreement was obtained for s in the range 1.0 to 1.2. However, their calculations based on the total number of particles in the events

observed (10^5 - 10^8) gave an average expected range of s from about 1.1 to 1.4. This discrepancy is probably related to the shower origin and propagation of energy via the N-component, and will be discussed later. They concluded that for showers whose total number of particles is on the order of 10^6, that if multiple cores exist they must lie within a radius of a few meters.

A similar experiment was performed at sea level by Fujioka[44]. He measured relative densities at distances from 5 to 47 meters from the core selector and recorded showers containing 10^5 to 10^7 particles. His data agree rather well with the theory of Nishimura and Kamata for s = 1.4 or 1.5.

A third experiment of this type was conducted at sea level by Haddara and Jakeman[45]. For their work they chose as a core selector a cloud chamber shielded by 5 cm of lead. They then identified cores by using the criterion that a cascade entering the cloud chamber should contain at least 9 particles. This corresponded to the presence of high energy photons or electrons, which in turn implied proximity to the core. Their results seem to give a good fit to the Nishimura and Kamata curve for s = 1.2. However, both their work and that of Fujioka are consistent with a smooth curve corresponding to s $\cong$ 1.3.

Another recent experiment in this range was undertaken by Kellerman, Shaw, and Walker[57] at 100 meters altitude. Using a "core selector and detector" device of shielded and unshielded counters, they found that more than 50 per cent of the cores could be located within 3 meters. Studying showers whose total number of particles varied from 5 x 10^4 to 5 x 10^5, they found agreement with Nishimura and Kamata for

$s = 1.25$ for all but the smallest showers, for which a value of s from 1.3 to 1.4 seemed to give the best fit. They concluded that, for $N < 5 \times 10^4$ electrons, the lateral distribution is no longer independent of shower size.

Next, the previous experiments conducted at large distances, i.e. $0.4 < \frac{r}{r_1} < 5$, will be discussed. Barrett, Bollinger, Cocconi, Eisenberg, and Greisen[46] used a hodoscope arrangement of counters located 1600 meters water equivalent underground in an attempt to locate the shower axis by observing the directions of μ-mesons. They found that by projecting the observed direction of the μ-mesons to the surface they could accurately determine the position of the shower axis. Four trays of unshielded counters aboveground completed the experimental setup. By noting that the counter tray which had the most counters discharged was always the one nearest to the shower axis, they concluded that there were no distinct, widely separated, multiple cores, the density decreasing smoothly with distance from the axis. They were also able to compute, using an assumed distribution function, the expected number of coincidences as a function of the distance from the axis. Their results agreed well with the Nishimura-Kamata distribution for $s = 1.4$ throughout their range of r from 50 to 500 meters.

In Russia, Zatsepin and his associates[37] observed showers at 3860 meters using a hodoscope arrangement of counter trays. They located the axis from the determination of relative densities as measured by their counters. Their results gave an electron density which varied as r^{-n} where $2.9 < n < 3.3$ for distances between 200 and 600 meters from the axis. This corresponded to showers whose age $s = 1.25 \pm 0.12$. However,

at their altitude they should have been observing showers at their maximum (s = 1). This may have been due to showers caused by successive groups of low energy photons created by the N-component cascade rather than by a single high energy photon.

During the last several years, there have been at least two large-scale experiments on air showers produced by very high energy primaries. First, there has been the work of Clark, Earl, Kraushar, Linsley, Rossi, and Scherb[55] at the Massachusetts Institute of Technology. Using plastic disk scintillators 105 cm in diameter, arranged in a circular array of about 460 meters in diameter, they have investigated the shower size, direction of the primaries, and the lateral distribution. They found no significant dependence of the lateral distribution on size or zenith angle. Also, their results agreed with the Nishimura and Kamata theory for s = 1.4 from 50 to 500 meters.

The second large-scale experiment was carried out at Harwell, England by Cranshaw, Galbraith, and Porter[56]. They used a triangular lattice of geiger counters, 1100 meters on a side and at 60 meters altitude, and were primarily concerned with the density distribution at distances greater than 100 meters from the axis. Their events had total numbers of electrons in the range 3×10^6 to 8×10^7 and their analysis showed agreement with Nishimura-Kamata for s = 1.4.

Finally, a resume' of the experiments conducted at small distances from the axis, namely for $\frac{r}{r_1} < 0.03$ will now be presented. This is the region of interest in the present experiment. Most of the experiments carried out in this region have been compared with the Moliere theory and have shown significant discrepancies.

Hazen[47] has studied the density distribution within a few meters of the core by using a cloud chamber at 3000 meters elevation. To select regions of high energy particles he used, in multiple coincidence, shielded counters below the chamber and an unshielded tray about two meters away. The high energy particles were identified by means of the showers they produced in the five one-inch lead plates within the chamber. That the events so selected were actually shower cores was supported by the fact that the counting rate agreed with the rate as found by Ise and Fretter[48] and by Blatt[49]. The analysis of these cores showed, on the basis of a Moliere distribution, that they were not as energetic as the total density of particles in the chamber seemed to indicate. In other words, the density gradients were much smaller than the Moliere distribution predicted. However, more recently, Relf[50] working at sea level with a large diffusion chamber observed several events whose axes seemed to be near the chamber and whose density gradients were consistent with the Moliere theory.

Williams[51] has measured the frequency of coincident bursts at 3050 meters altitude in two ionization chambers as a function of their separation to obtain a decoherence curve. His data were analyzed by Blatt[49]. The same experiment, as well as the same method of analysis, was also done at sea level by Campbell and Prescott[53]. In both cases the decoherence curve was flatter than that predicted by Moliere for separations less than five meters.

Using counters in a coincidence - anticoincidence array at 3260 meters, Kasnitz and Sitte[53] selected showers whose axes struck

close to a cloud chamber. A counter hodoscope was associated with the array to determine the shower density. They were thus able to determine the relative frequency of showers as a function of density and hence the variation of age with size. They found "s" to be a slowly varying function of the total number of particles.

Sitte, Stierwalt, and Kofsky[54], using five trays of unshielded counters connected to a hodoscope, were able to select showers whose axes fell close to the central tray. They then determined relative densities at about 2, 4, and 8 meters from the axis. By using additional shielded trays, they were able to determine the energy spectra of the photons and electrons and hence classify the showers into various age groups. Their data were difficult to interpret. The youngest showers should have had an age corresponding to $s = 0.8$, but the distributions agreed with the Moliere theory, which implies $s = 1$. The other age groups had almost identical distributions corresponding to $s = 1.2$.

Williams[51], and later Hazen, Williams, and Randall[17], with an assumed Moliere distribution function, were able to locate the shower axis by knowing the density at at least three ionization chambers. In principle, the ratio of densities between two of the chambers will determine a locus of possible shower axes and the ratio between the third and one of the others will yield another curve whose intersection with the first should locate the shower axis. Williams analyzed 28 events at 3050 meters elevation using this method and found consistent agreement with the Moliere distribution for showers of 10^6 - 10^8 particles. Hazen, et al., at 3260 meters, found that 80 per cent of their events agreed

with the Moliere distribution from 0.5 to 4 meters from the axis, but that at distances less than 0.5 meters a much flatter distribution was observed.

There have been two previous experiments employing essentially the same method as the present experiment, and which were designed to yield information about the lateral structure near the core. First, the work of Heineman[72] in which a multiwire chamber with twenty adjacent 4" x 18.5" collecting areas was used at 280 meters altitude. He was thus able to resolve the structure from twenty centimeters to two meters from the core. Fourteen events were analyzed in detail. These events seemed to indicate that a large percentage of showers have a total electron distribution which is as sharp as Moliere's within about fifty centimeters from the core, but which have a much flatter distribution at larger distances. There were also some showers that exhibited an almost flat distribution over the two-meter extent of the chamber and that were attributed possibly to multiple cores. Heineman concluded that multiple cores due to π°-decay-photons could not be resolved with his equipment.

Davis[75], in an attempt to improve and extend the work of Heineman, added two single wire chambers on either side of the large multiwire chamber. His resolution was no better than Heineman's, but by including the response of the side chambers the location of the shower axis was more accurately determined. Furthermore, by conducting the experiment at 3260 meters altitude a much larger number of events were recorded near the shower maximum. His results showed that over 80 per cent of the showers observed could be adequately fitted to the Moliere distribution. He also found about fourteen events out of the 9000 recorded that

showed some evidence of multiple core structure which was attributed to either multiple π^3 production in the first nuclear collision or contributions from later collisions of the N-component.

2.3 The General Problem Near the Shower Axis

The fact that the lateral distribution near the shower axis is sometimes flatter than that predicted by Moliere has often been attributed to multiple production of high energy secondaries at the shower origin. However, in view of the Nishimura and Kamata theory, all the experiments showing a flat distribution near the core can be satisfactorily accounted for by a consideration of the variation of the age parameter with distance, and need not be ascribed to spreading as a result of the initial interaction or N-component cascade. In fact, taking into account the nuclear origin of the showers, as well as the variation of s with r, it is hard to explain why the distribution near the axis is not flatter than observed. To explain the experimental evidence one must conclude that, at the origin of showers of 10^5 or more electrons, the most energetic photons and the N-component particles are contained in a cone whose half angle is less than 2×10^{-4} radians[23]. It must also be concluded that the particles in the N-component cascade that contribute appreciably to the soft component maintain a lateral distribution that has a strong peak within a few meters of the axis.

The difficulty in recognizing multiple cores may be due to the fact that at distances comparable to the supposed core separations the showers would be very old and hence would not have strongly divergent distributions. In an attempt to overcome this difficulty El-Mofty[58]

has recorded the decoherence curve of two ionization chambers under 5 and 7.4 radiation lengths of water. This experiment was inconclusive as to the existence of multiple cores but the coincidence rate was found to decrease strongly as the chamber separation was increased from 0.9 to 6.5 meters. Hazen[59] has made an analysis of El-Mofty's data and has shown that the theoretical decoherence curve, calculated for a pure single-cored electron shower, is not as steep as was supposed and is not in serious disagreement with the experiment. In addition, a number of the recorded coincidences were probably due to local showers produced in the water by the N-component.

2.4 Theoretical Considerations Near the Shower Axis

Since the soft component of the large air showers is undoubtedly of complex origin, the region near the axis should show some strucuture. The π^0 mesons, and other secondary particles that give rise to the soft component, should produce overlapping showers whose axes may or may not be resolved depending on the number of such secondaries of comparable energy, their average spacing, and the background effect of the nuclear cascade. In any case, the shower certainly should not have a single core of high density gradient. That is, one should find either multiple cores or a single diffuse core whose density is high but whose gradient is small. Since the effect of overlapping showers should produce a diffuse region at least as wide as that determined by the angular divergence of the initial N-component secondaries, a study of the lateral distribution near the axis should enable one to set limits on the angular divergence of the secondaries in the primary interactions. Calculations have been made[25], assuming

isotropic creation of the secondaries in the center of mass system, to determine the radius of the base of the cone containing secondaries of equal energy and uniform density. For single nucleon-nucleon collisions at high energies, these calculated radii were about five times too large to fit the observed distributions near the axes of large air showers.

It has been pointed out by Fermi[60], in connection with his statistical model of nuclear interactions, that conservation of angular momentum demands that, for non-central collisions between nucleons, the angular distribution of secondaries in the c.m. system cannot be isotropic. This decreases the theoretical value by a factor of about three, but this is still not enough to agree with experiment. Furthermore, it is applicable only to single nucleon-nucleon collisions. Complex collisions will, in general, result in a more nearly isotropic distribution of the secondaries.

A number of authors[61-63] have proposed modifications of the Fermi theory but the experimental evidence to date is not sufficient to enable one to make a choice. On the other hand, emulsion studies of high energy showers[64-70] have lent support to the unaltered Fermi theory and shown it to be fairly correct for these experiments.

2.5 The Method and Location of the Present Experiment

For this experiment a total of eight large, thin wall ionization chambers was employed. Three of these had a number of sensitive wires within the same chamber volume. These chambers will henceforth be referred to as multiwire or MW chambers as oppored to the remaining five single wire or SW chambers. Altogether, a total of 27 sensitive areas in the plane of observation were available, initially, for recording the number of shower

electrons passing through these areas. Later, these were reduced to 25 channels as explained in Section 3.2. All MW chambers were constructed of 1/16" aluminum which represents a thickness of 0.017 radiation lengths. The single wire chambers had walls of 1/16" galvanized iron representing a thickness of 0.089 radiation lengths. Now the recorded number of electrons in the chambers will be increased over the actual number in air above the chambers due to the transition effect. This effect is caused primarily by the materialization of photons as the shower electrons traverse the chamber walls. Bethe, as quoted in Williams,[51] has calculated the transition effect for a thin wall chamber. His formula indicates an increase in the number of electrons in the MW chambers by a factor 1.01 and in the SW chambers by a factor 1.15. This factor for the MW chambers is so nearly unity that the transition effect in these chambers was neglected for this experiment. The SW chambers were ultimately calibrated by means of showers which had a flat electron distribution over all the chambers (cf. Section 4.3) and then normalized to the density recorded by the MW chambers so that the transition effect for the SW chambers was automatically taken into account.

In Figure 1 is shown a plan view of the relative positions of the ionization chambers. The indicated dimensions of the chambers refer to their overall dimensions. All the showers discussed in Chapter V were recorded with this geometry. The presence of a skylight near the outside end of the left hand side chamber prevented placing a SW chamber at that position.

The experiment was conducted on the roof of the Randall Laboratory of Physics at Ann Arbor, Michigan, which is situated at an altitude of 280

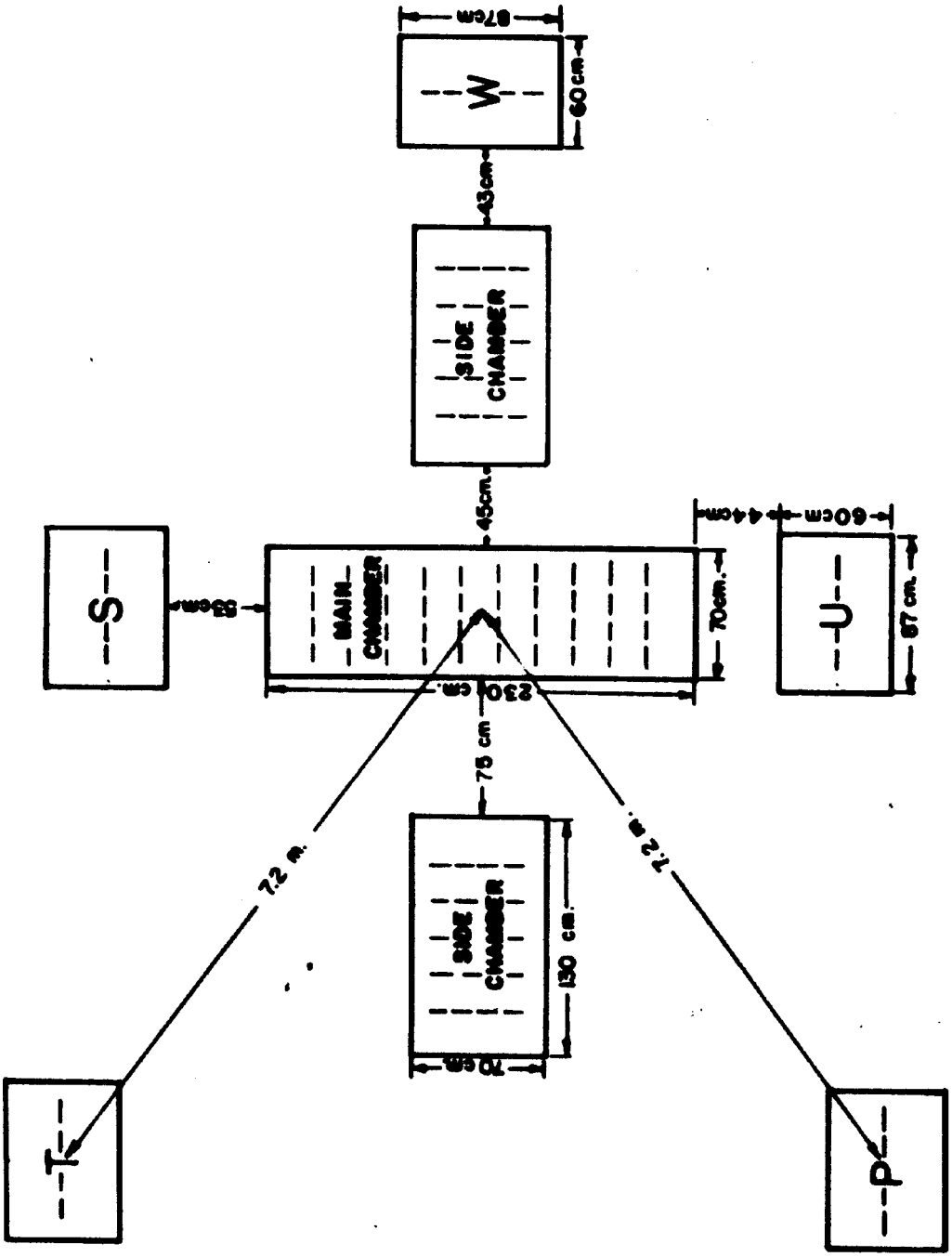


Figure 1. Plan View of Ionization Chamber Geometry.

meters and where for air, r_1 = 80 meters. A value of 37.7 gm/cm^2 has been used for X_o for air and 84 Mev for ϵ_o.[22] Since there are 997 gm/cm^2 of air above the observational level, the atmospheric depth is 26.4 radiation lengths.

CHAPTER III

EXPERIMENTAL APPARATUS

3.1 Introduction

In this section a general description of the experimental apparatus and its operation is presented. More detailed descriptions will appear in subsequent sections. A block diagram of the ionization chambers and associated electronics is given in Figure 2.

When the three geiger trays positioned under the main MW chamber were discharged within the resolving time of the coincidence circuit, there was a high probability that a shower had struck near the apparatus. Each shower electron produces ionization, electrons and positive ions, in the argon gas within the chamber. The collecting wires were at a high positive potential with respect to the chambers' walls and hence the ionization electrons are attracted to them. The resulting separation of electrons and positive ions induces a small negative change in the potential of the wires. These voltage pulses were amplified first by the preamplifiers located at the chambers themselves, and then by a final amplifying stage before being applied to the vertical deflection plates of the 28 cathode ray tubes. Accidental or chance coincidences could readily be recognized by a glance at the cathode ray tube display. If the event recorded were a true shower, then nearly every ion chamber channel should have a pulse displayed on it.

The coincidence pulse triggered univibrator I, whose positive going square wave was fed to a cathode follower and applied to the first grid of all cathode ray tubes, thereby turning on the beams. The negative

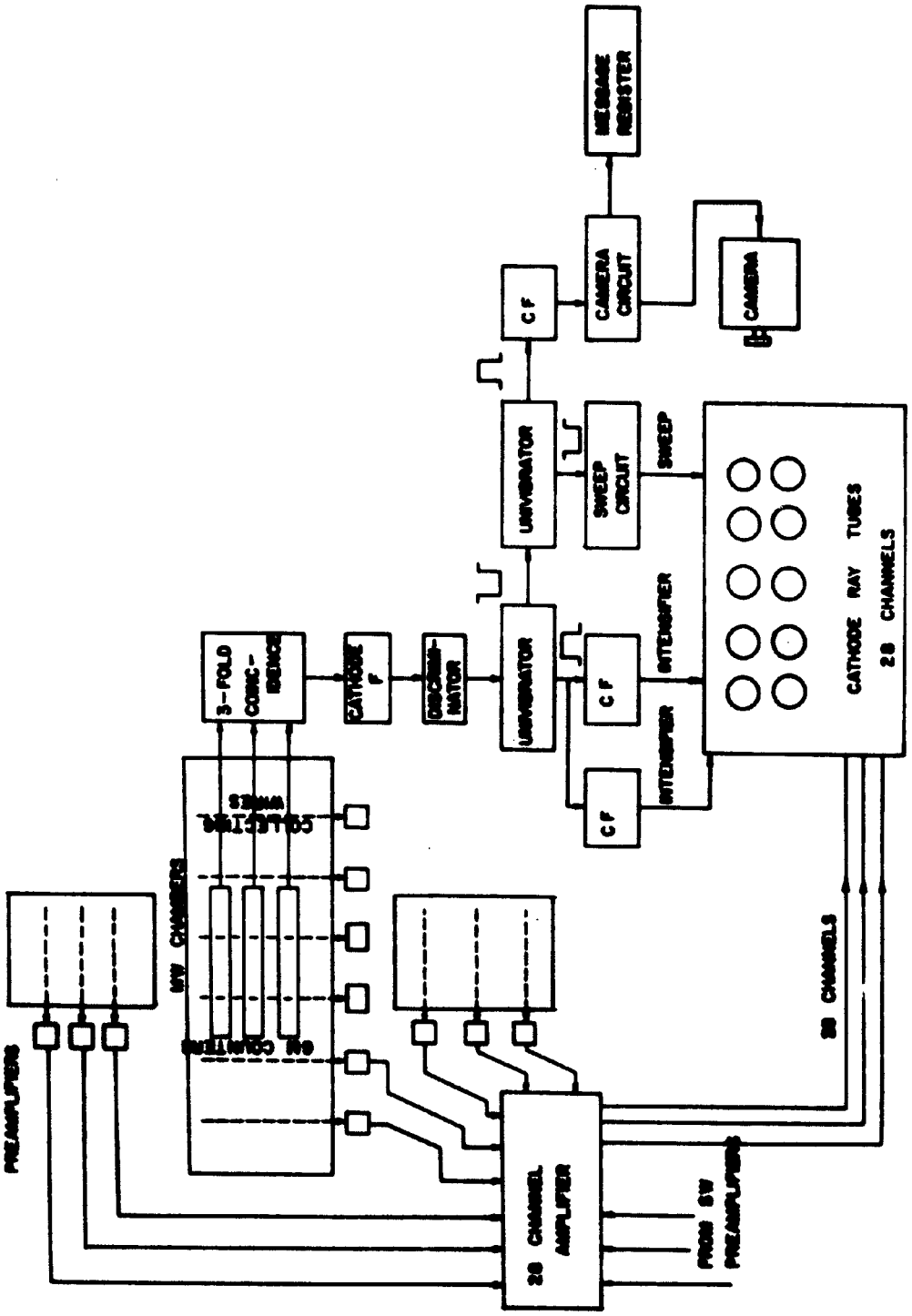


Figure 2. Block Diagram.

going square wave from univibrator I triggered univibrator II, whose negative going square wave was used as a clamp to start the sweep from the sweep circuit. The positive going square wave from univibrator II was fed to a cathode follower and then used to fire a thyration in the camera circuit. The camera circuit served two functions. First, it furnished power to an AC motor to wind the film to the next frame and second, it applied a voltage pulse to several argon lamps located in the plane of the cathode ray tube faces. Two of these lamps were used to illuminate an electric clock face so that a record of the time of each event appeared on film. Two more lamps which flashed through pin holes were used as fiducial markers by which to position the film for reading, a process to be described later.

In summary then, if a shower struck near enough to record a coincidence, the synchroscope was triggered and each ionization chamber pulse was amplified and displayed on the cathode ray tube faces. The complete display on all tubes was recorded on film and the camera was wound to the next frame awaiting the next event. The shortest resolving time between events was about one second.

3.2 The Multiwire Ionization Chambers

The main MW chamber had over-all dimensions of 7'8" x 2'4" x 8". The walls of the chamber were 1/16" aluminum. This chamber had 22 equally spaced nickel wires, 10 cm apart. The two end wires were dummies used to minimize end effects, i.e. capacitance between end wires and end walls. The collecting wires themselves were 0.024" in diameter and had a sensitive length of 19 1/2". Each wire was equipped with a cylindrical guard ring which extended inward 4 5/16" from the output side of the chamber and which

was electrically connected to ground. The opposite ends of the wires were connected to insulating plastic beads which were in turn fastened to phosphor-bronze springs to maintain tension and an additional 4 3/16" length of wire for support to the opposite wall. These supporting lengths of wire were electrically connected to the guard rings to preserve electric field symmetry. Since the MW chambers' walls were run at a high negative potential with respect to ground, it was necessary to shield the MW chambers completely by a grounded wire screen. The preamplifiers were also located within this shielding.

The original electrical connections for the collecting wires of the main MW chamber consisted of adjacent pairs of wires in parallel. Each parallel pair was then fed to a separate preamplifier. An exception to this scheme was that the two wires at each end of the main chamber represented four distinct channels and preamplifiers. Thus a total of twelve channels were available; eight of these had a sensitive area of 20 x 50 cm^2 and four had a sensitive area of 10 x 50 cm^2.

The side MW chambers had over-all dimensions of 4'4" x 2'4" x 8". These chambers had twelve wires apiece, the two end wires again being dummies. Except for the long dimension and total number of wires, the side chambers were identical in all respects to the main MW chamber. Again, adjacent pairs of wires were electrically connected together giving five 20 x 50 cm^2 channels for each of the side chambers.

In order to decrease the capacitance of the wires to ground and hence increase the signal-to-noise ratio, the following connections were subsequently made. Instead of connecting adjacent wires in parallel pairs, every other wire was connected electrically to the chamber wall.

This not only decreased the capacitance to ground for each channel but effectively isolated one channel from another, so that induction effects from adjacent collecting wires were completely negligible. The sensitive areas remained 20 x 50 cm^2. It was necessary, however, in order to maintain the same sensitive area for each channel, to reduce the number of channels in the main chamber to ten.

For calibration purposes, there were twenty Po-α sources plated on a copper rod which fitted inside a brass cylinder. This brass cylinder lay on the bottom of the main chamber along its long axis and had holes positioned under each wire so that a known amount of ionization could be deposited in the region of each wire. The side MW chambers were equipped with similar source rods. When not in use, these rods could be retracted into the brass cylinder which was thick enough to absorb all the particles, and hence no ionization was collected. These source rods were suitably altered at the same time the chamber connections were modified, so that sources were located only under collecting wires.

In addition to these calibration sources, there was a movable source in each MW chamber which was positioned directly under one of the sensitive wires. These source rods could be moved anywhere from the chamber wall to the wire and could also be retracted into a plate located under each chamber, in which position no ionization was collected. The purpose of these sources was to test for electron attachment, a procedure to be described later.

3.2.1 The Single Wire Ionization Chambers

The single wire chambers were constructed of 1/16" thick galvanized steel. They had over-all dimensions of

34 1/4" x 29 3/4" x 23 3/4". Originally there were six such chambers; one of them developed a leak and hence the experiment was conducted using the remaining five. The wires were 0.041" in diameter and had a sensitive length of 28 1/4". Guard rings 2 1/4" long, electrically connected to a 2 1/4" insulated length of supporting wire at the opposite end, were included on each chamber. The guard ring in each chamber was, in turn, connected to the collecting wire through a 5.6 megohm resistor. Since the walls of these chambers were run at ground potential while the wires were at a high positive potential with respect to ground, no external shielding was necessary.

A movable source rod was located perpendicular to one of the side faces of each of these chambers so that the Po-α source plated on the end of the rod could be positioned anywhere from the wall to the wire. These single source rods served the function of both types of source rods used in the MW chambers. Separate shielded "B" battery supplies furnished a potential difference of 1080 volts for both the SW and MW chambers.

3.3 The Argon Gas System

Since all the chambers were intentionally designed with thin walls in order to have a negligible transition effect, it was not possible to evacuate them, then fill with argon and seal them off. Therefore the following method, shown schematically in Figure 3, was devised.

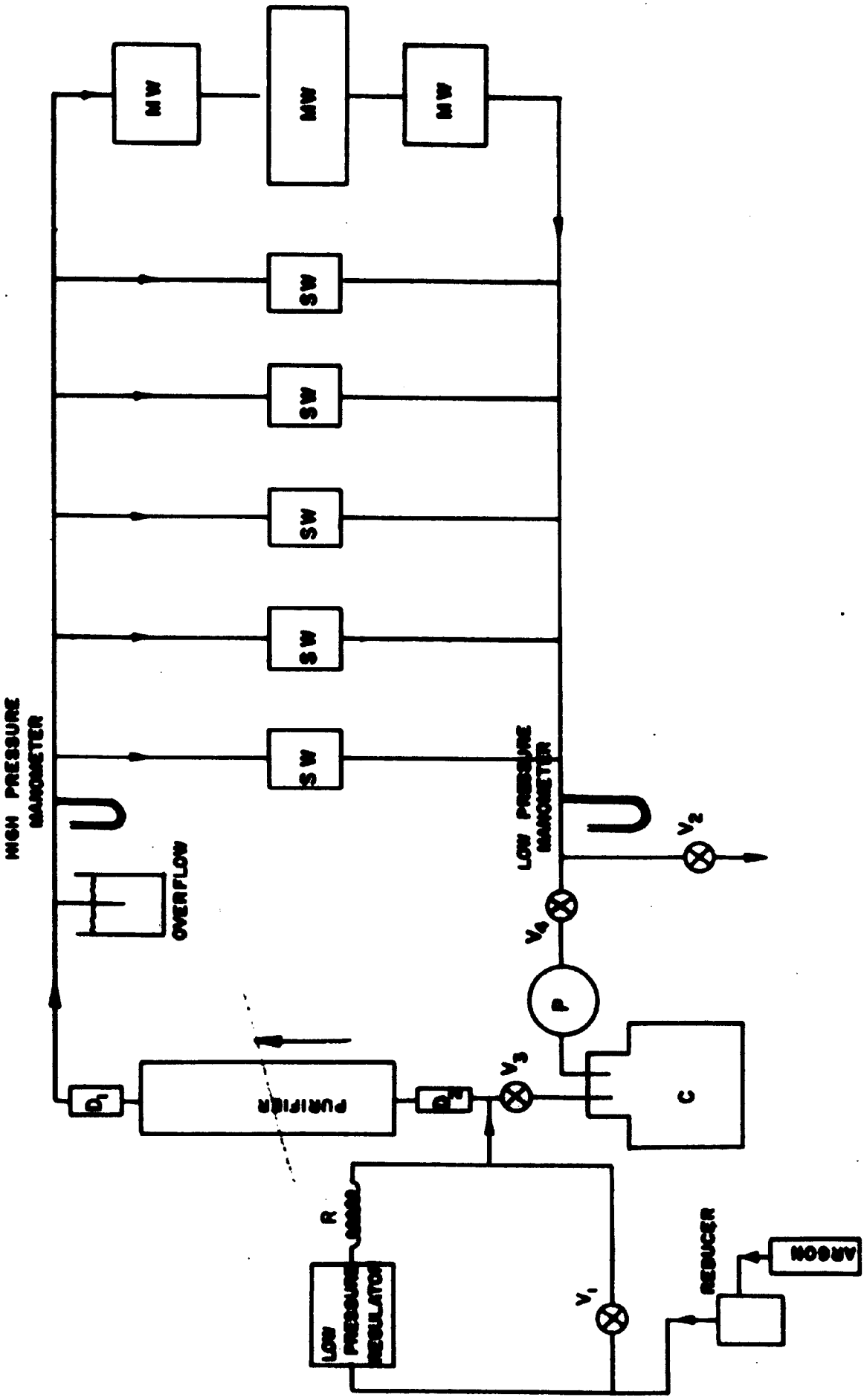


Figure 3. Schematic Diagram of Gas System.

The chambers were all connected via 1/2" plastic garden hose in a series-parallel combination as shown, such that each parallel branch had approximately the same flow impedance. The entire system was first flushed out with argon to displace most of the air. The system was then closed to the atmosphere and a continuous recirculation of the chamber gas through an oxygen purifier and two water-vapor traps was maintained. A complete description of the operation of the system and its component parts follows.

Cylinders of commercially pure argon (99.99 per cent) were employed. The cylinder pressure was reduced to about 18 psi and fed to the input side of a sensitive low pressure regulator. This regulator was designed so as to maintain a constant pressure at the output side. It admitted gas only on demand i.e. only when the system pressure, "felt" at the output side, fell below a certain preset level. D_1 and D_2 were brass cylinders 4" in height and 2 1/2" in diameter. They contained pellets of anhydrous $CaSO_4$, whose function was to absorb any water vapor that might be present.

The purifier was constructed from a pyrex tube, 64 mm in diameter and 40 cm long, which was filled with short pieces of copper wire. The tube was placed inside a cylindrical, electrically heated furnace which maintained a temperature of about 400°C. The function of the purifier was to remove oxygen from the system. The necessity for eliminating oxygen and water vapor had to do with the problem of electron attachment to be discussed in Section 4.4.

The pyrex tube could be removed from the furnace while in operation, in order to inspect visually for the presence of cupric oxide.

When nearly the entire length of the tube contained CuO, the complete assembly of furnace and tube were temporarily removed from the system. At the same time a stopcock on the low pressure regulator was turned off so that no argon entered the system while the purifier was absent. Hydrogen gas was then passed over the hot CuO, reducing it again to the metal. The flow of hydrogen was maintained for at least five minutes after the reduction was completed so that most, if not all, of the water formed in the chemical reaction was driven out the open end. The hydrogen was then flushed out with argon and the purifier was returned to the system.

A displacement-type pump P driven by an electric motor provided a continuous recirculation of the gas through the chambers, purifier, and desiccant, at a rate of about 20 cu ft/hr.

A means of protecting the chambers from mechanical damage due to excessive pressure, as a result of daily temperature increases or barometric pressure decreases, was necessary. This protection was accomplished by the overflow. This consisted of a tube which communicated with the system and was immersed in a fluid. Whenever the difference between system pressure and barometric pressure was greater than the depth at which the tube was immersed, excess gas merely bubbled out until the pressure was equalized.

In order to eliminate pressure surges due to the pump from being felt at the output side of the low pressure regulator, a filter R-C was included. R consisted of a coil of 3/8" - diameter copper tubing 48' long and C was a 3-gallon carboy.

Two open-end manometers filled with dibutyl phthalate, one at the high pressure end and one at the low pressure end, completed the gas system. Except for the argon cylinder, the chambers themselves and associated outdoor hoses, the entire system was located inside the same structure which housed the electronic equipment.

The system was operated in the following manner. Initially, the pump was off. Valves V_3 and V_4 were closed and V_1 and V_2 opened in order to flush the system. Valve V_1 allowed the low pressure regulator to be bypassed so as to obtain a fast flow rate while flushing, consistent with maximum tolerable chamber pressure. If complete mixing of the gases in the system is assumed, then the percentage of argon within the system after flushing with n volumes of pure argon will be $(1 - \frac{1}{2^n}) \cdot 100$ per cent. If n is ten, then the gas should be 99.9 per cent argon. Since the total volume of the system was about 100 cu ft, 1000 cu ft of argon were used to flush the system. The remaining oxygen was then removed by the purifier.

After flushing, valves V_1 and V_2 were closed and V_3 and V_4 opened. The pump was turned on and the low pressure regulator adjusted to maintain about two inches of water pressure about atmospheric at the low pressure manometer. At the normal pumping speed this produced a pressure about three inches above atmospheric at the high pressure manometer, which was two inches less than the maximum safe chamber pressure for which the overflow was set. This pressure margin was not sufficient to compensate completely for daily pressure changes due to temperature variations and, in general, there was some gas lost through the overflow during the day and some gas admitted to the system via the regulator and purifier

during the night. The lowest pressure point in the system, however, was always kept positive with respect to the atmosphere so that no air could enter the system through possible small leaks.

3.4 The Amplifiers

In Section 4.2 it is shown that the voltage pulse appearing on a particular wire is directly proportional to the number of shower electrons passing through the sensitive volume of that wire. Since there are large variations in shower size, i.e. total number of electrons, and further since electron densities per wire may vary widely in a single event, non-linear, high gain amplifiers were employed. These amplifiers were designed by Heineman[72] for a previous, similar experiment and are described in detail in the above reference. They had a rise time of about two microseconds and were calibrated daily, as explained in Section 4.2.1, to detect any changes in their characteristics. Most of the amplifiers were stable, but owing to the frequent calibrations small changes could be detected and corrected for. A typical amplification curve is shown in Figure 4. Each of the preamplifiers had a potentiometer in its feedback circuit which could vary the gain by a factor of three while still maintaining some feedback at maximum gain. The frequency response was practically independent of gain setting. The tubes (6AK5's) were selected for low noise and microphonics. In addition, each preamplifier had its filament voltage to the first stage dropped by a ten-ohm resistance. It had been found by Driggers[74] that this increased the noise-free tube life.

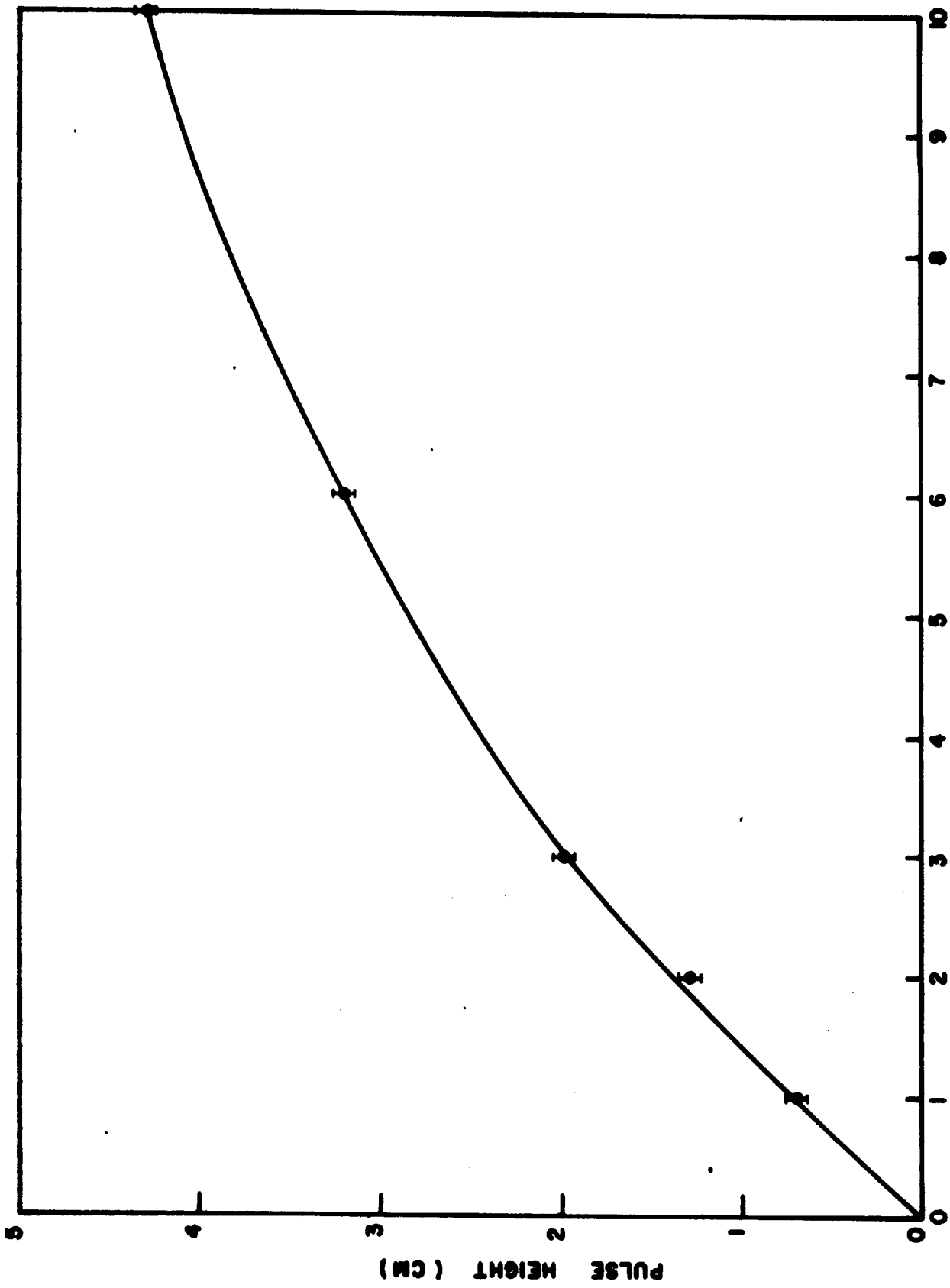


Figure 4. Amplification Curve.

Two 300-volt regulated power supplies were available, each supplying plate voltage for half the preamplifiers. An R-C filter circuit was included in each preamplifier to decouple it from the supply. The last stage of each preamplifier was a cathode follower which was connected via a coaxial cable to the back of the synchroscope chassis, upon which the non-linear last stages of amplification were mounted.

The operation of the cathode ray tubes demanded, as explained in Section 3.7, that the amplifiers have a low frequency cutoff as low as possible and yet compatible with no microphonics, low frequency oscillations, or 60-cycle pickup. The shortest time constant was 700 microseconds, the coupling of the preamplifiers to the last stages. Since the voltage pulses induced on the central wires decayed with a time constant of about 1400 microseconds, the pulses appearing on the cathode ray tubes had an undershoot. The method used to measure pulse heights in the absence of a base line reference is discussed in Section 3.10.

Although the amplifiers were non-linear, occasional large showers did drive some of the amplifiers beyond saturation. In order to have some idea of the correct voltages corresponding to these pulses, each calibration included pulser voltages well beyond the saturation voltage. Since a "fast" sweep speed was employed on the synchroscopes, for the recording of showers as well as for the amplifier calibration pictures, the increase of pulse <u>width</u> with amplifier input voltages beyond saturation became a measurable parameter.

In order to reduce 60-cycle pickup, the filament voltage for the tubes in the preamplifiers was supplied by a 6-volt storage battery. The battery was charged continuously by two 6-volt, 10-ampere full-wave rectifiers. To further reduce the 120-cycle fluctuations arising from the battery chargers, a large L-C filter was included.

3.5 The Geiger Counters

Because of its relative simplicity, geiger tube triggering was employed. Three trays, each 30 inches in length and each covering a sensitive area of 350 cm^2, were constructed. The high voltage was supplied by dry "B" batteries. The three trays were located about one foot below the main chamber, parallel to each other and to the long axis of the chamber. The distance between trays was 30 centimeters. It was found that this geometry gave a high probability ($\sim$ 90 per cent) for three-fold coincidences due to small showers whose axes were within a meter of the array, as well as a higher probability of triggering for larger showers.

3.6 The Coincidence Circuit

The three-fold coincidence circuit was of the conventional type due to Rossi. It had a measured resolving time of 50 microseconds. No pulse shaping networks were found to be necessary and the geiger tube outputs were fed directly to the grids of the coincidence circuit.

3.7 The Synchroscopes

A general description of the operation of the synchroscopes has been given in Section 2.1. The controls included focus, intensity

astigmatism, and horizontal and vertical positioning. It was found that only one of each of the foregoing controls was necessary to adjust properly all 28 channels. However, two independently adjustable "brightener" voltages, from two cathode followers driven by univibrator I, were available for pulsing the first grids of the cathode ray tubes. This was necessary since it was not possible to find 28 tubes whose beam cut-off voltages were sufficiently close. Thus two groups of similar tubes were used.

Other synchroscope controls were potentiometers for adjusting the pulse length of the univibrators and a switch used to introduce two different sweep speeds. A "fast" sweep speed of 200 microseconds was employed when recording showers and when pulsing the chambers, and a "slow" sweep speed of 800 microseconds when recording α - pulses. The reason for the "slow" speed is pointed out in Section 4.2.2.

The cathode ray tubes themselves were 5-inch Dumont 3GP1's. They were mounted in a closely spaced rectangular 4 x 7 tube array. Although green phosphor cathode ray tube screens are usually poor for photographic purposes, they were rendered practicable in this experiment by applying accelerating voltages about 30 per cent above the tube ratings as well as by utilizing slow pulses and writing speeds. The latter was the reason for the long time constants in the amplifiers, as referred to in Section 3.4.

The negative high voltage for the cathode ray tubes was supplied by a half-wave rectified, R-C filtered supply. The primary winding of the high voltage transformer was operated from a constant voltage transformer so that its output would be stable with respect to line voltage variations.

It was found that for long periods (~ 1/2-1 hour) between events, enough light from the cathode ray tube filaments showed through the tube faces to cause a large diffuse black spot on the film at the center of each cathode ray tube. This trouble was reduced to a satisfactory minimum by decreasing the filament voltage. A variac supplied 80 volts A C to the primary of the filament transformer, effectively diminishing the visible light intensity from the filaments without appreciable loss of beam intensity.

3.8 The Camera

A 35-mm camera was constructed, using a Zeiss Sonnar f/1.5 lens, to photograph the cathode ray tube array. The same voltage pulse applied to the argon lamps was used to operate a message register in the focal plane of the camera. Thus each frame had an identifying number. There was also a message register in the plate circuit of the thyratron to see if the camera was recording the proper number of events, as well as to check the coincidence rate. Kodak Linograph Ortho 35-mm film was employed throughout the experiment. This is a fast film which has a high sensitivity in the green region of the spectrum and low sensitivity in the red.

3.9 The Precision Pulser

A means of pulsing the chambers with known voltage pulses was necessary for amplifier calibration. An MIT model pulser was modified so as to produce pulses whose frequency characteristics were similar to ionization pulses. A precision attenuator and rotary switch enabled

pulses in the millivolt range to be applied to the chambers in the ratios 1:2:3:6:10:20:40:90. It was not necessary to know the absolute voltage scale since the quantity of interest, i.e. total number of electrons per channel, involves the ratio of shower voltage pulse to α-particle voltage pulse (cf. Section 4.2).

All chambers were pulsed simultaneously and recorded photographically for each of the pulser attenuator settings. The MW chambers were pulsed by applying the pulser voltage to the chamber walls, while the SW chambers had their wires individually pulsed. The shape of the output pulses from the pulser were made to correspond to ionization pulses from the MW chambers. Since the collection time, and hence the rise time, of ionization pulses from the SW chambers was about three times as long as for the MW chambers, a series R-C network was used to further shape the pulses being applied to the SW chambers.

3.10 The Film Reader

To facilitate the reading of pulse heights from the film, an optical projecting and enlarging device was constructed. This consisted of a 35-mm film strip projector whose beam was doubly reflected by plane mirrors to provide a path length corresponding to a magnification of about 18. The reflected beam was then incident upon the under side of a specially constructed transmission screen. This screen was made by affixing two thicknesses of 3-mil frosted plastic sheeting to a transparent plane glass plate. It was found that the quality of the resulting image on such a screen was superior to that obtained by using commercial ground glass. A third thickness of frosted plastic was supported by a

separate rectangular wooden framework which was placed over the screen and actually formed an integral part of it. This framework was free to be moved in a plane parallel to the fixed screen and was held in any desired position relative to it by a pair of permanent magnets. All three plastic sheets were in intimate optical contact so that no parallax was encountered.

It was pointed out in Section 3.4 that, owing to the undershoot of the pulses, the quiescent base lines from which pulse heights are to be measured could not be determined accurately from the same frame on which the pulses were recorded. This difficulty was overcome by first recording on film several frames of "blank" sweeps, i.e. with no signal applied to the vertical deflection plates. These were the quiescent base lines. The pinhole images of the argon lamps provided reference points on each frame which were fixed relative to the blank sweeps. The image of the positions of the base lines and the reference points were then drawn permanently upon the movable screen. When reading pulse heights the movable screen was adjusted so that the permanent reference points coincided with those on the frame under consideration. Pulse heights were then measured from the permanent base lines to the tops of the pulses. At the beginning of each daily film strip, blank sweeps were recorded to serve as a check against possible base line drift. However, no base line drift was detected.

CHAPTER IV

THE EXPERIMENTAL METHOD

4.1 The Principles of Ionization Chamber Operation

When electrons and positive ions are created within the chamber their separation produces a current which induces a voltage change between the central wire and chamber walls. It will be assumed here that there is only one central wire in the MW chambers. The effect of neighboring wires has been calculated by Heineman[72] and shown to be negligible. Rossi and Staub[71] have analyzed the time dependence of the voltage appearing across a high resistance between the central wire and ground of an ionization chamber. Their method and results will be outlined briefly.

If R is the resistance between the central wire and ground, and C is the capacitance between central wire and ground, then the amplifier input voltage V appearing across R is

$$V(t) + RC \frac{dV(t)}{dt} = RI(t), \qquad (1)$$

where it is assumed that $V = 0$ when $t = 0$. The current I(t) will depend on the number of ion pairs formed.

There are three possible cases that may be considered here, depending on the magnitude of the time constant $\tau = RC$ relative to the collection times of electrons T^- or positive ions T^+. The collection times will depend on the chamber geometry the potential difference between the electrodes, and the gas pressure. For the MW chambers $T^- \approx 8$ microseconds and $T^+ \approx 8$ milliseconds. Due to the longer path lengths, the

SW chambers had collection times of $\sim 24 \times 10^{-6}$ seconds and $\sim 24 \times 10^{-3}$ seconds for electrons and positive ions, respectively. But for either type of chamber $T^- \ll \tau \ll T^+$, so that the electron current is integrated by C while the positive ion current is not affected. The electrons have all been collected by the time T^- while the positive ions have not moved appreciably from their point of formation. Under these conditions the chamber is said to be operating as an electron pulse chamber. The other two cases occur when $\tau \ll T^-$ and T^+ and when $\tau \gg T^-$ and T^+. It would appear that the latter case would be the most desirable since the voltage pulse would then be directly proportional to the number of ion pairs formed, irrespective of their points of formation. However, its long resolving time prohibits its use in investigating single cosmic ray events.

For the present case of the electron pulse chambers, the first term in Equation (1) may be neglected for $0 \leq t \lesssim T^-$, since

$$V(T^-) \ll \frac{I}{T^-}\left[V(T^-) - V(0)\right].$$

In this approximation Equation (1) reduces to

$$\frac{dV(t)}{dt} = \frac{1}{C} I(t).$$

Upon integrating from t = 0 to t = t, the following expression is obtained:

$$V(t) - V(0) = \frac{Q(t)}{C}, \text{ where}$$

$$Q(t) = Q^-(t) + Q^+(t) = \int_0^t I^-(t)\, dt + \int_0^t I^+(t)\, dt.$$

$Q^-(t)$ and $Q^+(t)$ may be considered to be the charges induced on the central wire by virtue of the presence of electrons and positive ions, respectively.

The integration of the currents with respect to time yields the following results:

$$Q^-(t) = \frac{e}{U} \sum_{i=1}^{N_o} \left[U_i^-(t) - U_i(0) \right]$$

and $Q^+(t) = \frac{-e}{U} \sum_{i=1}^{N_o} \left[U_i^+(t) - U_i(0) \right]$.

Here, $U_i(0)$ is the potential at the position of formation of the ith ion pair and $U_i^-(t)$ and $U_i^+(t)$ are the potentials at the positions of ith electron and positive ion, respectively at time t. N_o is the total number of ion pairs and e is the electronic charge. The assumption has been made here that the presence of ionization in the chamber will not affect the field. This is certainly true in this case since the chamber potential $U \cong 1000$ volts and is thus very large compared to $V \cong 10^{-3}$ volts.

Now, since all the electrons have been collected by time T^- while the positive ions have not moved appreciably since formation, the above expressions for the induced charges become for $t = T^-$

$$Q^-(T^-) = \frac{e}{U} \sum_{i=1}^{N_o} \left[0 - U_i(0) \right] = \frac{-e}{U} \sum_{i=1}^{N_o} U_i(0)$$

and $Q^+(T^-) = \frac{-e}{U} \sum_{i=1}^{N_o} \left[U_i(0) - U_i(0) \right] = 0.$

Thus, the voltage pulse appearing on the central wire rises to a value $V(T^-) = \frac{1}{C} Q^-(T^-)$ and then decays with a time constant $\tau = RC$.

It can be seen that $V(T^-)$ depends on the position of formation of the ion pairs, so that it would seem difficult to obtain any quantitative information. However, the assumption is made for this experiment that the

shower electrons will produce an approximately uniform distribution of ionization in the chamber. Therefore, by integrating U over the chamber volume, an average voltage may be found at which all ion pairs may be said to be formed. The maximum voltage pulse V appearing on the central wire may then be written as

$$V = \frac{Q}{C} = \frac{e}{CU} \sum_{i=1}^{N_o} U_i(0) = \frac{e N_o}{C} \frac{\bar{U}_i}{U} = \frac{e N_o}{C} f \qquad (2)$$

The ratio of average potential to total potential f will depend on the chamber geometry, i.e. the potential distribution. These factors have been calculated in Appendix A and are shown there to have the values 0.93 for the SW chambers and 0.92 for the MW chambers. This value for the MW chambers pertains only to the potential distribution resulting after the changes that were made in the MW chamber connections referred to in Section 3.2. The "f" factor applicable to the original MW chamber connections has been calculated by Heineman[72] and shown to be equal to 0.87.

4.2 Method of Calibration

The assumption will now be made that every shower electron passing through the chamber gas produces the same number of ion pairs N_o. Then the total voltage pulse produced by N shower electrons will be

$$V = \frac{N N_o e f}{C} .$$

The number of ion pairs produced by a single electron may be written as $N_o = j l \delta$, where j is the average specific ionization for an electron in argon in ion pairs/gm/cm^2, l is its path length in centimeters, and δ is the density of argon in gm/cm^3. In order to find V in terms of N_o,

it is necessary either to know the value of C or to introduce a known amount of ionization in the chamber. Since the capacitance is difficult to measure or calculate, the latter method was employed in the present experiment. The number of ion pairs formed in argon by an alpha particle has been shown[75] to be proportional to its energy. Thus, if W_o is the energy dissipated in the formation of one ion pair, then $\frac{E_\alpha}{W_o}$ will be the total number of ions pairs formed. E_α is the energy of the α-particles, and in this case was equal to 5.3 Mev, since Po^{210} was used as the α-particle source.

Now, for the MW chambers, the α-particle sources were located at the bottom of the chambers in a low field region but they do have a finite range of about 5 cm in argon at atmospheric pressure. Since the potential within the MW chambers changes appreciably within this distance from the wall, and since the specific ionization of an α-particle varies along its path, an f factor for α-particles f_α was calculated as shown in Appendix B and resulted in a value of 0.98. Then the voltage pulse produced by an α-particle $V_\alpha = e(\frac{E_\alpha}{W_o})\frac{f_\alpha}{C}$. For the SW chambers, whose sources were also located at the wall for the α calibration, it was assumed that the potential was constant over this range and hence $f_\alpha = 1$.

By eliminating the capacitance C between the above equation and Equation (2) Section 4.1, an expression for the total number of electrons passing through the sensitive volume of a particular wire is obtained.

$$N = \frac{E_\alpha}{j18W_o}\left(\frac{V}{V_\alpha}\right)\left(\frac{f_\alpha}{f}\right) \qquad (3)$$

From theoretical considerations and experimental evidence[22] it is believed that the energy W_o per ion pair is independent of the

ionizing particle. Then it can be said that jW_o is the energy dissipated by collision by a shower electron in argon.

Since the ionization loss for relativistic electrons is practically independent of their energy, a close approximation to the collision loss of every shower electron can be obtained by assuming every electron to have an average energy of 100 Mev[21]. It is conceivable that some of the secondary electrons produced in the chamber by collision will have energies so high that they will not dissipate all their energy within the chamber volume. However, the collision probabilities being about the same in air as in argon, for each such electron leaving the chamber there will be on the average another entering the chamber, having been produced in air above the sensitive volume. Also, since any electrons produced by collisions are not counted in the shower function $N(E_o, 0, t)$, they should not be counted in the chambers. This means that the ionization produced by each electron and all its secondaries should be counted as if due to only one shower electron. Then jW_o represents the total collision loss for electrons of energy 100 Mev. This was calculated from equation (1.12) in Rossi and Greisen[21] to be 2.1 Mev-gm^{-1}-cm^2. This quantity may also be calculated by another method. Since the total average energy loss per radiation length for shower electrons is $\epsilon_o N(E_o, 0, t)$ [22], then the energy loss per gm-cm^2 per electron is merely $\frac{\epsilon_o}{X_o} = \frac{84}{37.7} = 2.2$ Mev-gm^{-1}-cm^2.

Using the latter value for jW_o, the following expressions for the probable number of electrons passing through the sensitive volume of a particular wire were calculated.

$$N_{MW} = 72.2 \frac{V}{V_\alpha} \quad \text{for MW chambers } (\ell = 20 \text{ cm})$$

$$N_{SW} = 24.3 \frac{V}{V_\alpha} \quad \text{for SW chambers } (\ell = 60 \text{ cm})$$

4.2.1 Amplifier Calibration Procedures

Because the amplifiers used in this experiment were non-linear, it was necessary to calibrate their output pulse heights in terms of their input voltages. By applying a voltage pulse to the walls of the MW chambers from the pulser, a voltage $V' = \frac{C_c}{C} V_{cal}$ was induced on the central wires, where C_c is the capacitance of the collecting wire or wires to the chamber walls and V_{cal} is the output voltage of the pulser applied between chamber walls and ground. C is the total capacitance of the central wire to ground including the grid to ground capacitance in the first stage of the amplifier. It is not necessary to know the absolute values of either C or C_c but only that they remain constant, so that the α-particle pulses for multiples of V_α can be related to h_α, the deflection of the cathode ray tube beam for α-particles.

The calibration procedure then consisted of plotting for each channel the pulse heights h for the various pulser voltages V_{cal} (cf. Figure 4). Then the pulse height for an α-particle h_α corresponded, from the curve, to a voltage $V_{cal\alpha}$. Now the voltage appearing at the grid of the first amplifier tube when collecting ionization due to α-particles is $V_\alpha = \frac{Q_\alpha}{C}$, and $V_{cal\alpha} = \frac{Q_\alpha}{C_c}$ is the pulser output voltage corresponding to α-particle pulse height h_α. Similarly, for showers, if the voltage at the grid of the first tube is $V = \frac{Q}{C}$, then the corresponding $V_{cal} = \frac{Q}{C_c}$ which can be determined from the curve, knowing the pulse height h. The ratio $\frac{V_{cal}}{V_{cal\alpha}}$ is then equal to $\frac{Q}{Q_\alpha}$

which is in turn equal to $\frac{V}{V_\alpha}$, assuming that C and C_c do not change. This ratio was then inserted in Equation (3).

The calibration technique was slightly different for the SW chambers. Here the pulser voltage was introduced at each chamber, via a 1200 μμfd capacitance, onto the grid of the first amplifier stage. A similar analysis shows that the ratio $\frac{V_{cal}}{V_{cal\alpha}}$ is again equal to $\frac{V}{V_\alpha}$.

For the pulser calibration the synchroscope was triggered by the pulser output so that pulses appeared on all channels simultaneously at the beginning of the sweep. Two frames for each of the eight pulser settings were photographed daily and used to plot the amplification curves and maintain a continuous check on their reproducibility.

4.2.2 The α-Particle Calibration

To photograph the α-particle pulses, the pulser was placed on a fast repetition rate and the synchroscope on the "slow" sweep speed. Exposures of approximately one to two seconds duration were taken, the synchroscope being rapidly triggered by the pulser output. About ten frames were usually recorded in this manner, the camera being tripped manually after each exposure. The resulting pictures therefore included a large number of α-particle pulses appearing at random across the sweep. This explains the purpose of the "slow" sweep; namely, to obtain a large number of α-particle pulses in a short exposure time.

Now, not all the α-particle pulses were the same height due to finite thickness of the sources and due to the probability of one pulse riding on the tail of another. The first effect will always decrease the pulse height and the second effect may cause either an increase or decrease. However, the probability of an increase is much less than that for a decrease since the undershoot of the pulse is much longer than the pulse itself. The pulse height h_α was then determined by drawing a line across the tops of the maximum visible pulse heights, ignoring the few rarely occurring large pulses. The same technique was followed for each channel.

4.3 The Electron Attachment Problem

Electron attachment is the process whereby a free electron attaches itself to a heavy molecule, forming a negative ion. In the electron pulse chambers any electrons so captured before reaching the collecting electrode will result in a decrease in pulse height from the true value, since the lower mobility of the heavy negative ions increases the collection time by a factor of about 1000. Thus, once captured, they will no longer contribute to the total voltage pulse.

Only certain gas or vapor molecules show an affinity for electron capture. Among those that do not are H_2, N_2, and the noble gases such as argon. The principle molecules, in the present experiment, that do have a finite probability for attachment are O_2 and H_2O. The method employed for the removal of these contaminants has been discussed in Section 3.3.

The usual criterion for determining freedom from attachment has been to insure that the chamber potential was above that for pulse height saturation. Driggers[74] has suggested that this is not a valid criterion, and indeed his work and that of Heineman[72] and Davis[75] has supported this conclusion. The method employed by these three authors, as well as the method used in this experiment, is the following. A polonium α-source was plated on the end of a movable grounded copper rod. Each SW chamber was equipped with such a rod which was fed through an O-ring seal into the chamber in a direction perpendicular to the chamber wire. In each of the MW chambers one such source rod was positioned under one particular wire. These sources could then be moved anywhere from the wall to the wire.

If attachment is present, the pulse heights, due to the ionization produced by these sources, should increase as the sources are moved toward the wire. This is so because the collection path length for the electrons will be decreased and hence the probability for electron capture before collection will be decreased. In fact, if no attachment is present, there should be a slight decrease as the source is moved toward the wire since the ionization is being released in regions of lower and lower potential. Of course for distances the order of the α-particle range, widely varying pulse heights should be observed and indeed this was found to be the case. The main point, however, is that there is no reason to expect an <u>increase</u> in pulse height in the <u>absence</u> of attachment as the source is moved from the wall toward the wire.

In practice no attachment was evident in the MW chambers but the gas in the SW chambers continued to show a small amount of attachment

even after many hours of purification. This was believed to be caused by the evolution of gaseous contaminants from the soldered seams and joints inside the chambers. The rate of evolution was apparently greater than the argon flow rate through the chambers or at least complete mixing was not being achieved. Since the seams in the MW chambers were all welded this problem for them did not arise. Consequently, it was felt that the α-particle calibration for the SW chambers would not be reliable. As an alternative means of calibration a number of showers that exhibited a flat electron distribution over both the SW and MW chambers were analyzed, so that the voltage pulses from the SW chambers could then be normalized to the density as determined by the MW chambers. In the next section (4.4) all references to the α-calibration pertain to only the MW chambers.

After several days of continuous recirculation and purification the chambers were tested for lack of electron attachment. When no attachment was indicated in the MW chambers, a saturation curve was taken for each type of chamber. These curves are reproduced in Figures 5 and 6. They show the relative pulse height as a function of chamber potential. Frequent checks on these curves showed no significant variations throughout the experiment.

4.4 Experimental Errors

The statistical fluctuations in the recorded number of electrons N_1 passing through the sensitive volume of a particular wire are expected to be at least as large as $\sqrt{N_1}$. Since the total error is the square root of the sum of the squares of the individual errors, any errors which depend on N will be neglected if they contribute less than $\frac{1}{3}\sqrt{N}$ to the total error.

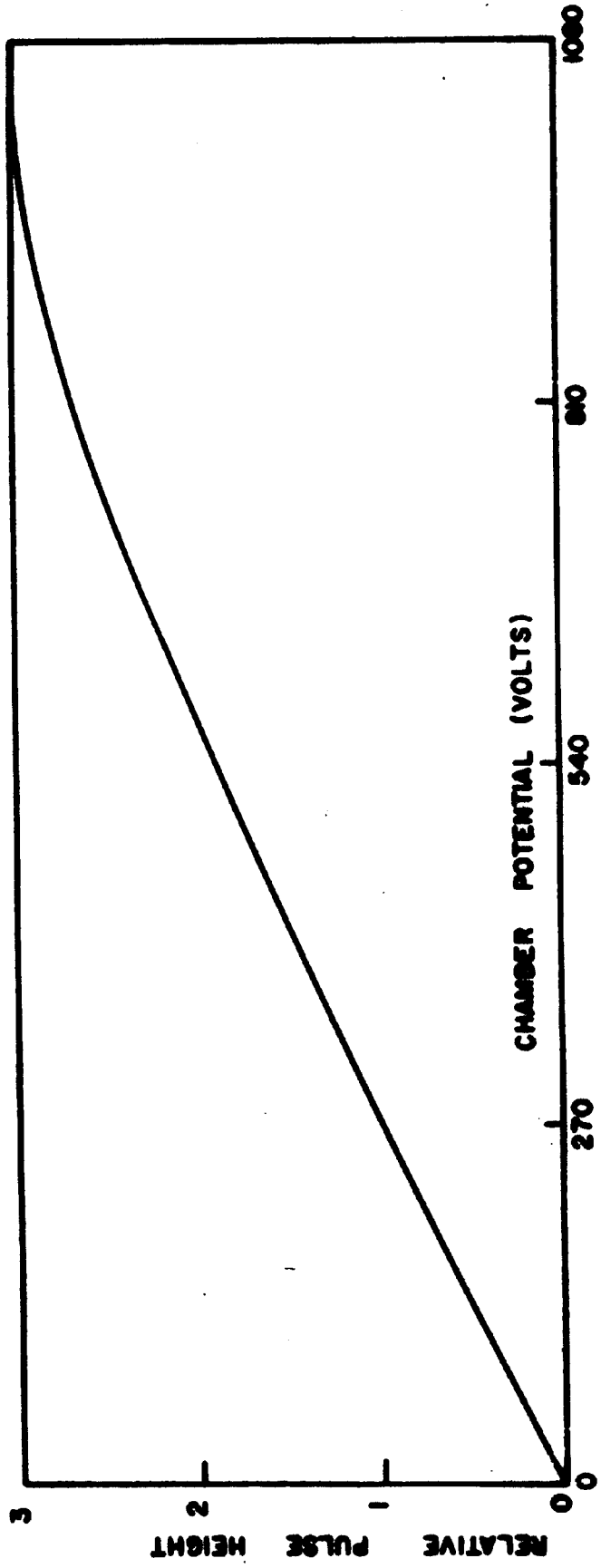


Figure 5. Saturation Curve for [illegible] Chambers.

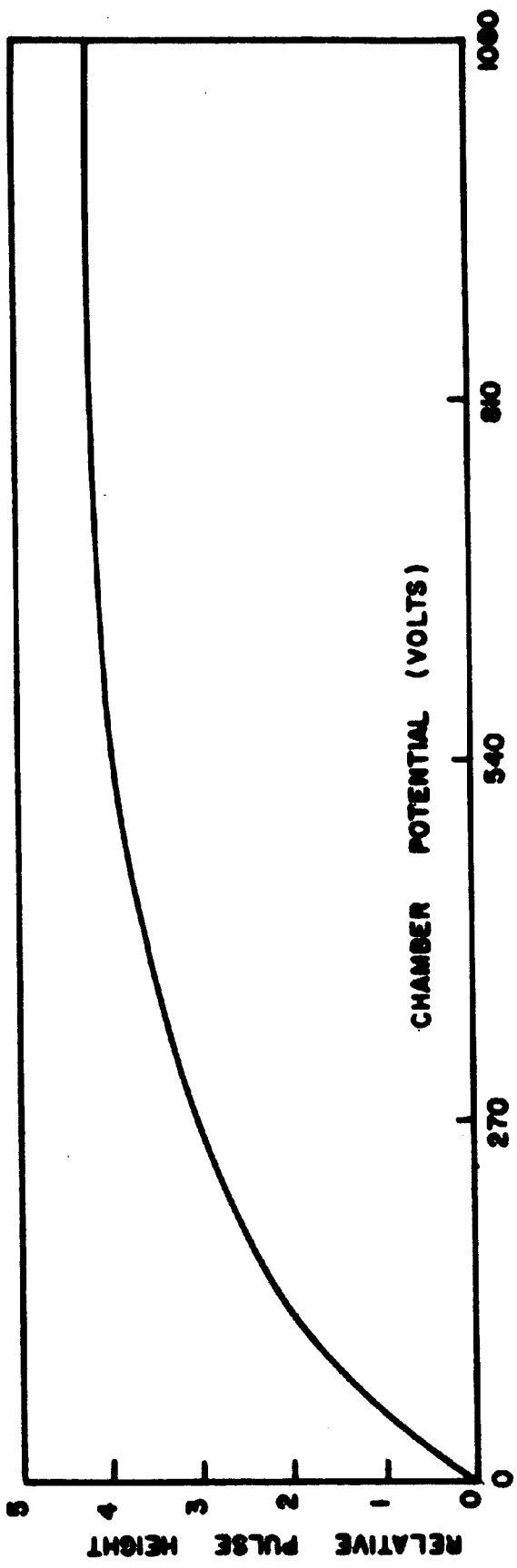


Figure 6. Saturation Curve for [illegible] Chambers.

Most of the showers recorded had a maximum N_1 of about 30 electrons giving an error of about 18% due to statistical fluctuations. Thus any errors less than about 6% can be disregarded for $N_1 \leq 30$.

Random errors in the α-calibration are evidenced in the reproducibility of $V_{cal\alpha}$. From calibration to calibration the average deviation of $V_{cal\alpha}$ for a single channel was about 6.0% and the average deviation of each channel from the average in a particular calibration was about 2.3%. The rather large error in the former case is probably due to an uncertainty in judging which one of several α-particle pulse heights to measure. These differing pulse heights are attributed most likely to the fact that the α-particle sources were not collimated and that the chamber potential distribution changed appreciably within a distance perpendicular to the wall equal to the α-particles' range. The differences in α-particle pulse heights for a particular channel did indeed correspond to errors of the order of 5%. The deviation of each channel from the average in a particular calibration was found to be systematic and hence was attributed to an actual variation of capacitance from channel to channel.

The random errors occuring in the measurement of individual pulse heights due to finite width of the trace or due to inaccuracies in measurement may be investigated by comparing independent pulser calibration pulses. The average difference for one channel from one calibration to the next was 0 to 1/4 mm. This error is negligible compared to statistical fluctuations for pulse heights from about 2mm up to within a few mm of the saturation value ($\sim$4 cm).

In summary then it will be assumed that all experimental errors are negligible compared to statistical fluctuations for pulse heights $\geq$ 2 mm up to saturation height and for channels whose recorded number of electrons is $\leq$ 30. For the few events in which some or all of the data do not lie within these limits, the additional appropiate errors have then been included.

CHAPTER V

METHOD OF ANALYSIS AND INTERPRETATION OF EXPERIMENTAL RESULTS

5.1 Ionization Chamber Theoretical Response Curves

In order to compare the experimental results with the theoretical predictions of Nishimura and Kamata, the finite sensitive areas of the individual detectors must be taken into account. Three sets of theoretical response curves were calculated numerically from Equation (1) Section 2.1.2 for s = 1.2, 1.3, and 1.4. These curves show the predicted number of shower electrons passing through the sensitive volume of each wire in the main chamber (or side chambers if x and y are interchanged) for showers whose axes passed near to or through the chambers. A typical set, for s = 1.4, is presented in Figure 7. The coordinates of the shower axis are designated by x and y according to the rectangular coordinate system shown in Figure 8. In Figure 7 the abscissa represents distances in centimeters along the y-axis as measured from the y-coordinate of the shower axis while the parameter is the x-coordinate of the shower axis. The ordinate indicates the number of electrons per 20 x 50 cm^2, this being the sensitive area of a MW channel. These curves were calculated for showers whose total number of electrons N is 10^5. Since the theory of lateral spread indicates that relative densities are independent of shower size to a good approximation, the ordinate was plotted logarithmically to facilitate the determination, of shower sizes other than 10^5 when attempting a graphical "fit" to the experimental data as explained below.

Most of the showers selected for analysis in this experiment exhibited a peak of maximum density somewhere along the y-axis of the main

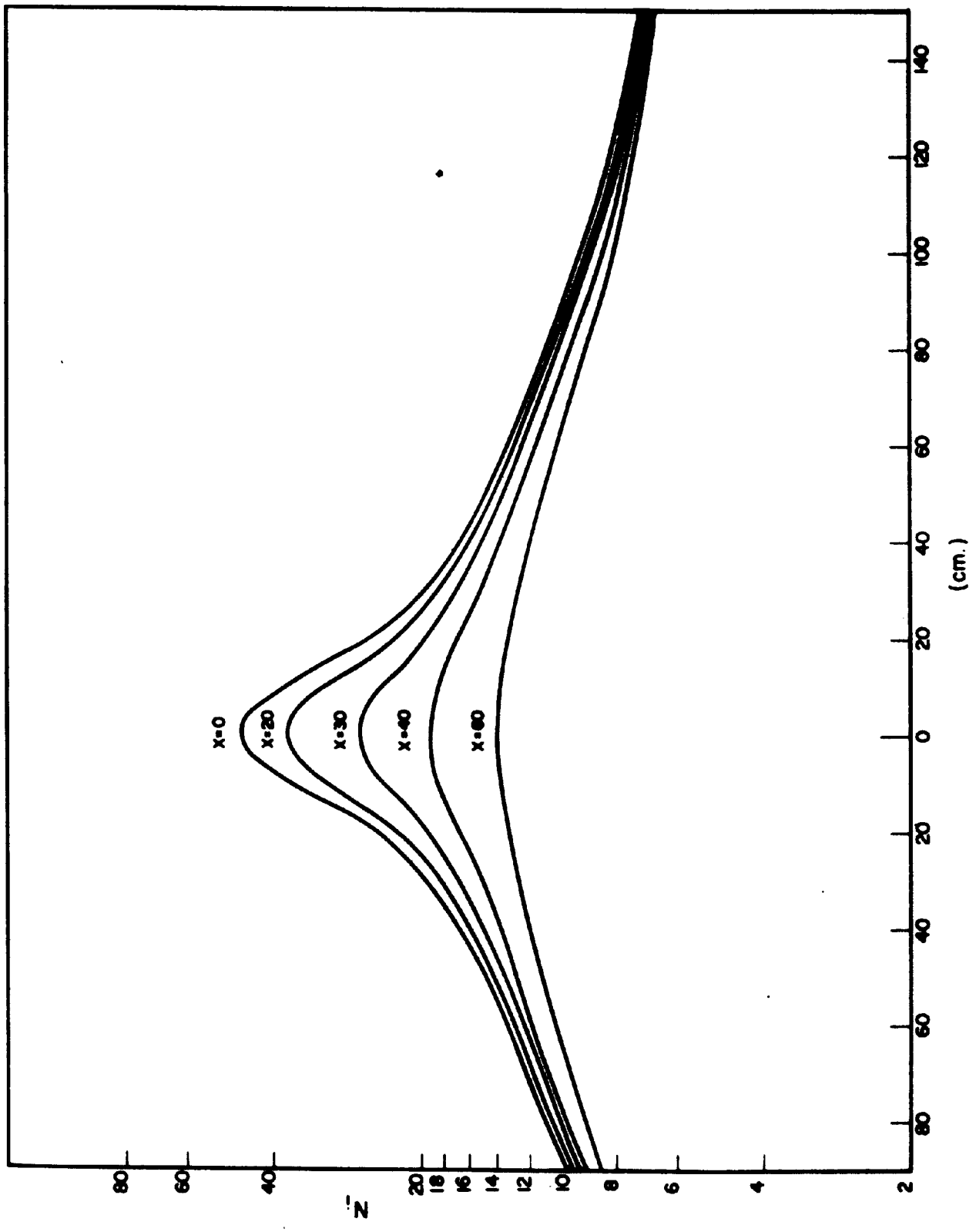


Figure 7. Ionization Chamber Response Curves for s = 1.4, N = 10^5

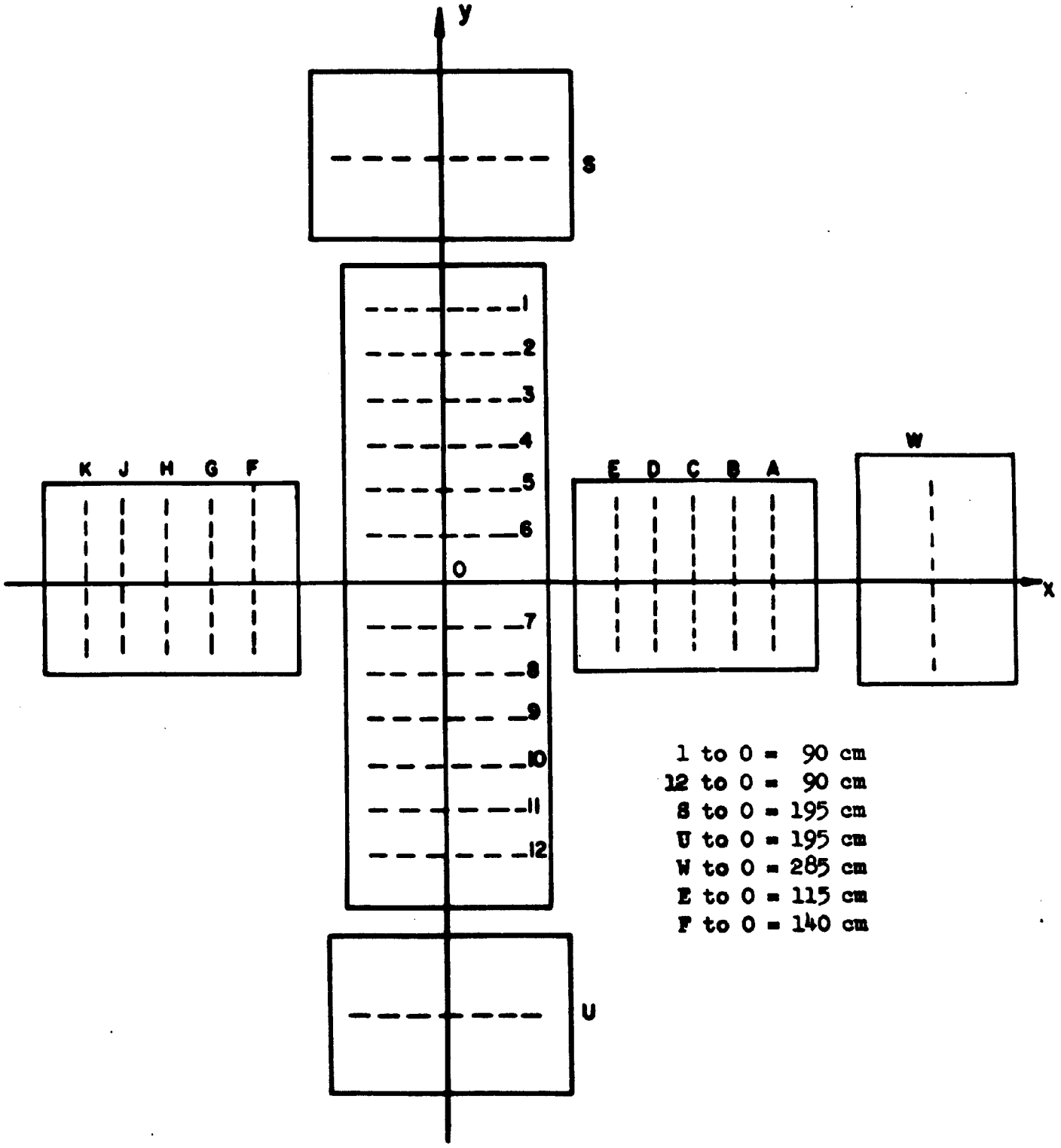


Figure 8. Coordinate System in Observational Plane.

chamber. This then determined the y-coordinate of the shower axis. The experimental data were also plotted semilogarithmically to the same scale so that by superimposing the theoretical curves a "best fit" could be obtained by varying x, y, N, and s. In some cases these four parameters did not uniquely determine a fit. An examination of the side chambers' and single wire chambers' responses usually resolved this ambiguity.

5.2 Systematic Deviations from the Response Curves and Fluctuations

The lateral distribution function of Nishimura and Kamata is based on single-particle initiation of cascade showers. The discussion in Chapters I and II has indicated that many large air showers are superpositions of showers having various energies and produced at various depths in the atmosphere. Thus the experimental lateral distribution could be expected to show multiple maxima as well as being less steep near the axis then for single-cored showers. If multiple maxima are to be resolved, the separate cores must have comparable energies and be separated by at least two wire spacings or forty centimeters. If either condition is not satisfied the resulting distribution will merely appear flatter than for a single-cored shower.

Another reason for expecting departures from the theoretical response curves is that the theory has treated only the average behavior of showers while, in reality, statistical fluctuations from the average will certainly be encountered. If a probability function, proportional to the lateral distribution function for electrons of energy E, $P_r(E, r, s)$, could be used to describe the manner in which all electrons of this energy

were independently distributed over r, then a Poisson distribution could be used to describe the expected number of particles passing through a given channel area for a given sized shower. The rms fluctuation in that number would be just the square root of the average number. Now it is certainly true that the shower particles are not independent so that fluctuations about the average would be expected to be larger than Poissonian. This problem of fluctuations has been investigated by Heineman[72]. He concluded that for showers where $N \geq 10^4$ the dependency existing between the individual particles will not (except in rare cases due to one single large-angle scattering) significantly increase the fluctuations about the average number of electrons $\bar{N}_i$ per channel. Thus, these fluctuations may be adequately represented by $\sqrt{\bar{N}_i}$. In the presentation and interpretation of actual cosmic ray showers all data are therefore displayed with standard deviations of $\sqrt{N_i}$ except as noted in Section 4.3.

5.3 The Selection of Individual Events for Analysis and Method of Presentation

Many of the showers that triggered the coincidence circuit had axes sufficiently far removed from the MW chambers that the density of particles was essentially constant over the extent of the array. Several of the larger of these "flat" showers were analyzed for the purpose of calibrating the SW chambers as pointed out in Section 2.5 and Section 4.3. The events selected for an analysis of the lateral distribution near the core were those that exhibited evidence of a peak in any of the MW chambers. The triggering arrangement, however, had a bias in favor of showers whose axes hit nearest to the main chamber. Most of the showers selected for

analysis had a total number of electrons between about 3×10^4 and 3×10^5.

In presenting the results all experimental data are plotted semilogarithmically with the proposed theoretical curve or curves superimposed on the data. Most of the events are fitted to the main chamber's response since the ten to twelve closely spaced channels in the main chamber are statistically more favorable for analysis. The side chambers' responses, and/or corresponding curves based on the main chamber fit, are shown to the same scale in the same figure so that each event is illustrated in two dimensions. The number of electrons recorded by the SW chambers (with the exception of T and P) was normalized to the sensitive area of one wire in a MW chamber and included graphically on each diagram. The theoretical responses of chambers T and P, which were located about seven meters from the origin (cf. Figure 1), were not included in general unless their experimental responses were non-zero. In those cases the above information is presented numerically on the appropriate drawings.

The main chamber's wires are numbered consecutively from positive to negative y and the side chambers' are lettered from positive to negative x as shown in Figure 8. (Note the omission of letter "I").

It should be pointed out that a minimum of about six electrons per channel usually did not result in a measurable signal so that unless otherwise indicated an experimental result of zero electrons does not necessarily mean that N_i is equal to zero for that channel. This minimum measurable level is indicated by a horizontal line at $N_i = 6$ on each figure.

As explained in Section 3.2., the MW channels did not always have the same sensitive area throughout the experiment. Whenever events were

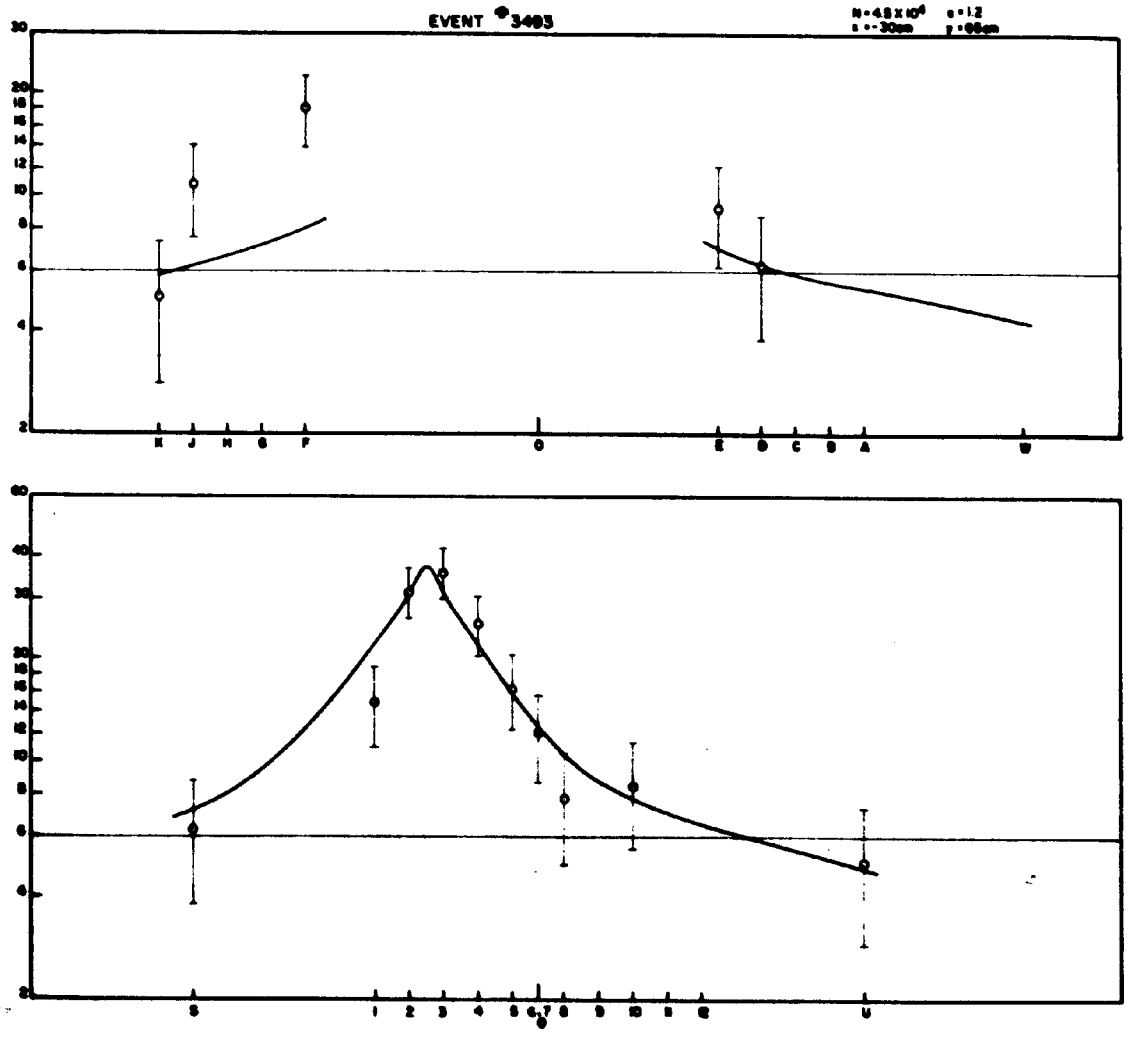

EVENT #3493
N=4.8x10⁶ s=1.2
x=-30m y=96m
K J H G F O E D C B A W
S 1 2 3 4 5 6 7 8 9 10 11 12 O U

Figure 9.

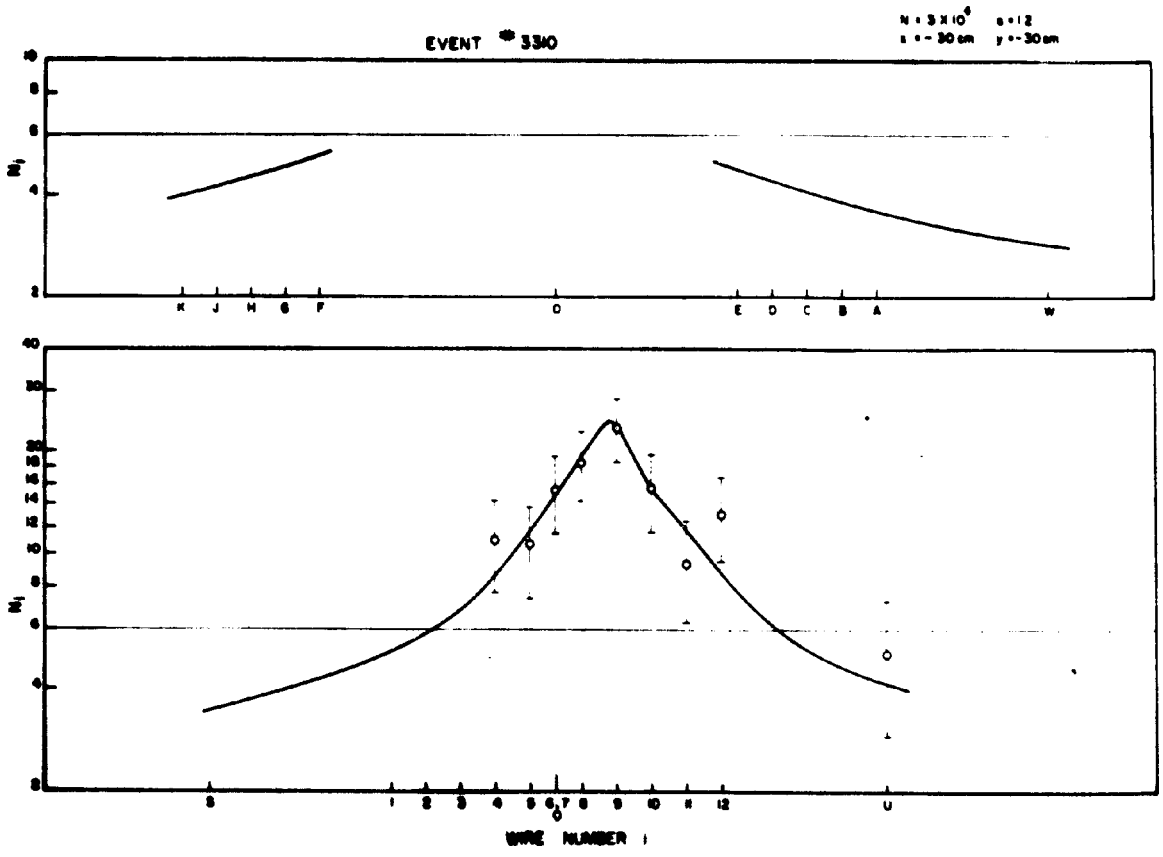

EVENT # 3310
N = 3 X 10^6
x = -30 cm
y = -30 cm
K J H G F
D
E D C B A
W
S
1 2 3 4 5 6 7 8 9 10 11 12
U
WIRE NUMBER

Figure 10.

recorded in which adjacent pairs of 10 x 50 cm^2 channels were encountered, the data for these channels were averaged and plotted as single points.

Complete agreement between experiment and theory requires that the theoretical curves must pass through at least two-thirds of the error flags on the average and that the experimental points themselves must lie at random on either side of the curve.

5.4 Individual Events and Their Interpretation

In this section a sample of the events recorded and selected for analysis will be presented. In most cases the proposed theoretical fit or fits are superimposed on the experimental data. If agreement seems unsatisfactory an attempt is made to discuss possible reasons for disagreement. For "bookkeeping" purposes the events are referred to by their actual message register numbers appearing on the film and bear no other significance.

Event #3495 is shown in Figure 9. This event was fitted by a response curve for $N = 4.5 \times 10^4$, $s = 1.2$, and shower axis located at $x = -30$ cm and $y = 65$ cm. No pulses were recorded on channels 9, 11, and 12 in the main chamber. Channel 9 could have had as few as 6 electrons and still have the top of its flag fall on the curve. The side chambers and SW chambers are all in good agreement with the fitted curve.

Another excellent fit was obtained in event #3510, Figure 10. The fitted curve was for a shower of age $s = 1.2$, whose axis hit at $x = -30$ cm and $y = -30$ cm, and which had a total of 3×10^4 electrons. No side chamber responses were recorded which explains why x was chosen to be -30 cm instead of $+30$ cm. Had x been equal to $+30$ cm then channel

E should have indicated 7.8 electrons. This number of electrons per channel is usually detected whereas for x = -30 cm both channels E and F are at the threshold of detectability. Of course, the presence of fluctuations really precludes making such a choice at all in this case. However, this serves to illustrate the method employed in general. The predicted responses of channels 1, 2, and 3 are also consistent with the minimum measurable densities.

The next event is shown in Figure 11. Again, a best fit is obtained for a shower where s = 1.2. The fitted curve indicates a size corresponding to 4.2×10^4 electrons and with an axis at x = 40 cm, y = 50 cm. Channel K has the only experimental point out of 25 channels that does not fall on the curve within the limits of statistics. There is no doubt that the theory correctly describes this shower at these distances from the axis.

Event #4006 was the smallest shower recorded, having $N = 2.25 \times 10^4$ electrons. This event is shown in Figure 12. The y-coordinate of the shower axis was chosen at 40.5 cm, but the x-coordinate could have been at either +20 cm or -20 cm. Once again excellent agreement is achieved for a shower whose age corresponds to s = 1.2.

The statistics in event #3635, Figure 13, were not as good as they might have been since channels 9 and 10 were inoperative at the time and 1 and 2 evidently had too few electrons to yield a measurable pulse. On the basis of the six channels that did show pulses, a fit was proposed where $N = 5 \times 10^4$ and s = 1.3. The shower axis appears to lie along the y-axis of the main chamber and 30 cm from the center. No pulses were recorded on the side chambers or SW chambers, a result that is compatible with the fitted response.

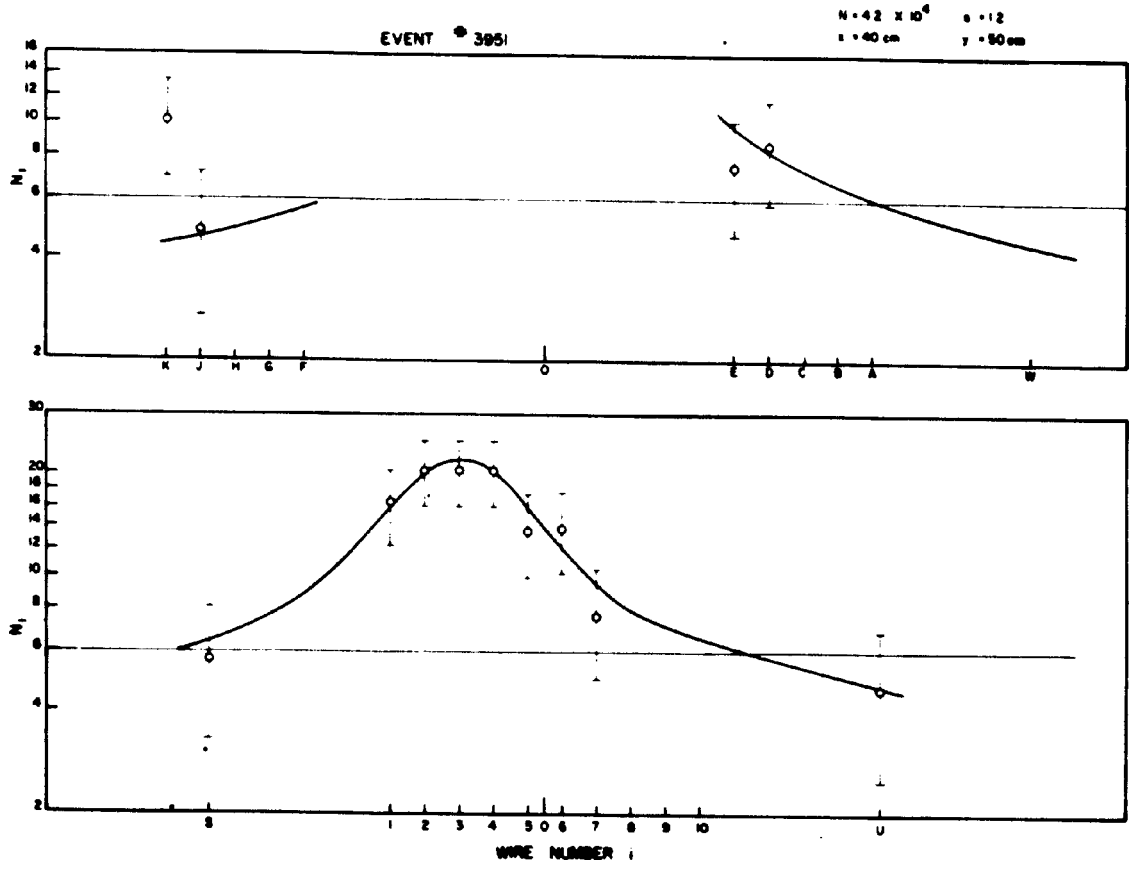

EVENT 3951
N = 4.2 X 10^6
s = 12
x = 40 cm
y = 50 cm
N_i
K J H G F
O
E D C B A
W
S
1 2 3 4 5 6 7 8 9 10
U
WIRE NUMBER i

Figure 11.

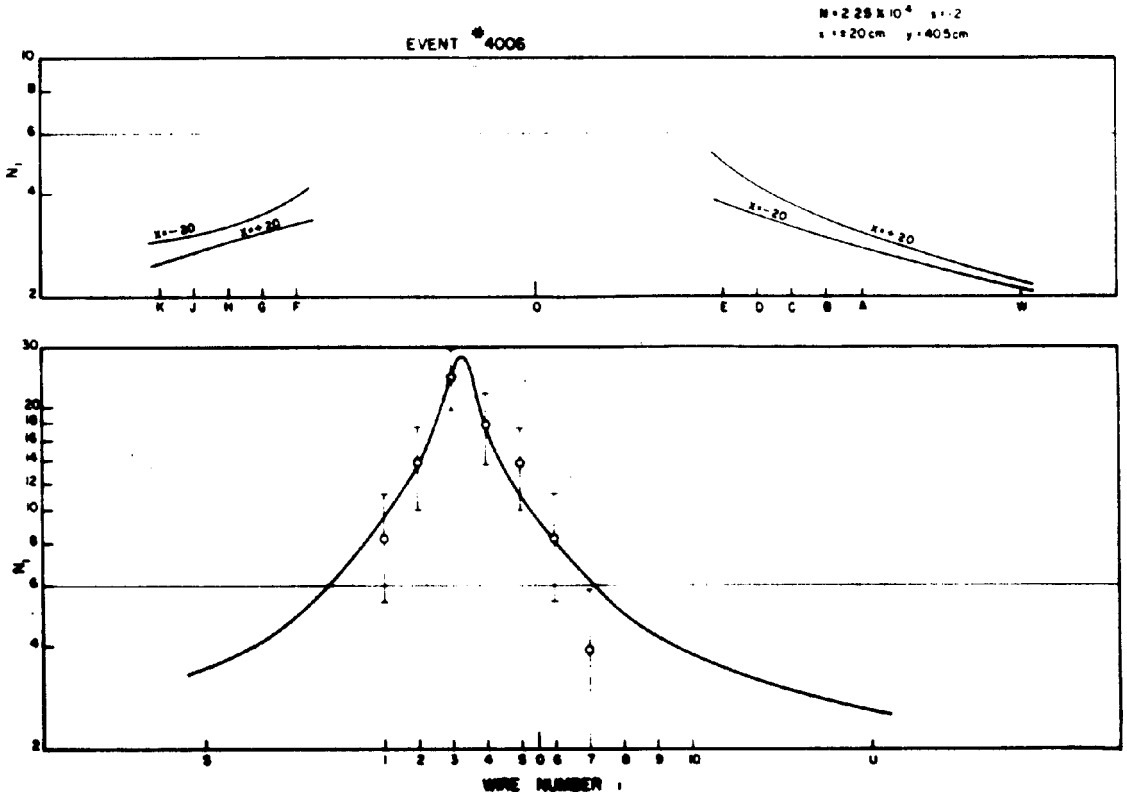

EVENT #4006
N = 2.28 X 10⁴ s = 2
x = ±20 cm y = 40.5 cm
x = -20
x = +20
K J H G F
O
E D C B A W
WIRE NUMBER

Figure 12.

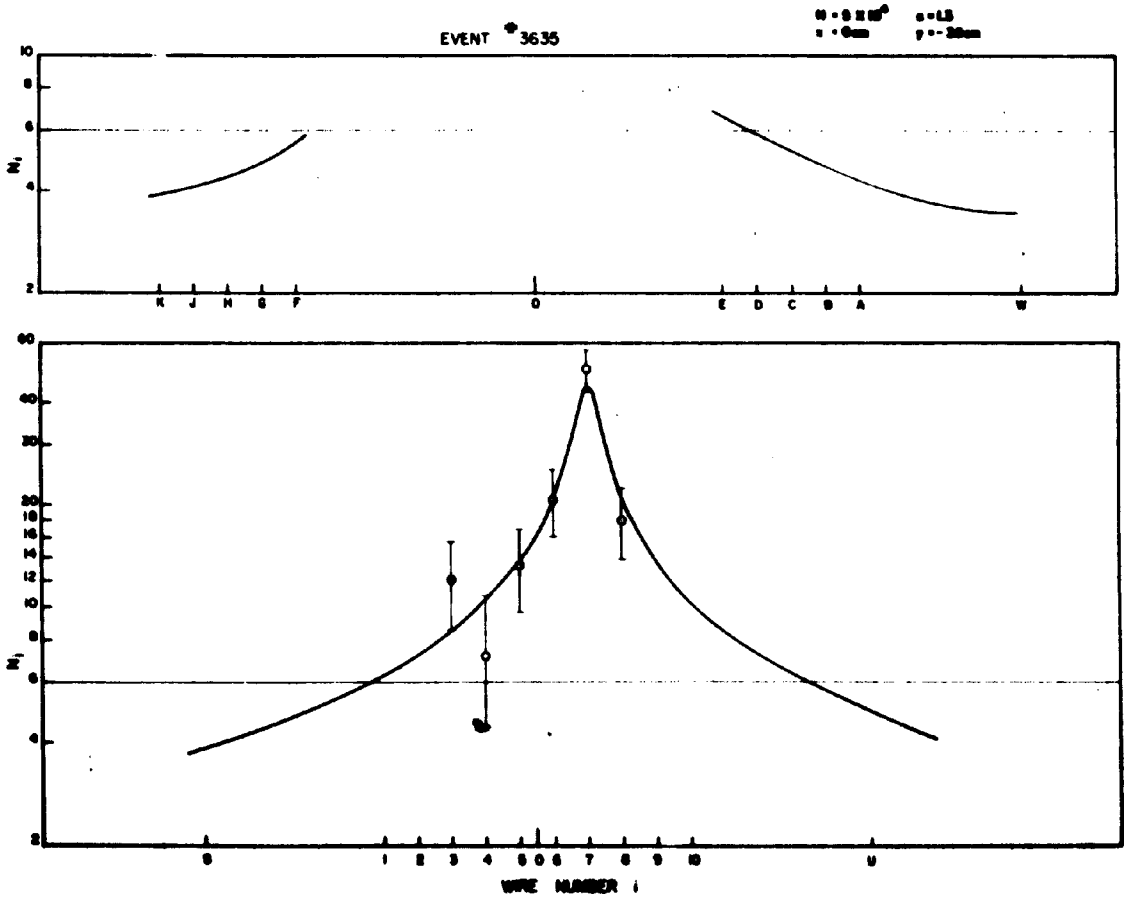


Figure 13.

Another event with s = 1.3 is shown in Figure 14. Here a satisfactory fit was obtained with $N = 4.5 \times 10^4$ and with the shower axis located at x = 20 cm, y = -30.3 cm. Channel 9 was not functioning when this event was recorded and no signal was measurable on channel 1. The only other channel having a signal was E which was too high by less than one standard deviation. Overall, the fit seems to be very good.

The next event (Figure 15) is presented with two proposed fits. The upper curve is for a shower of 3.84×10^4 electrons and whose axis is at x = 30 cm, y = -35 cm. The corresponding age parameter is 1.2. A second fit was proposed for s = 1.4 and is shown by the lower curve. This response predicts 7×10^4 particles when the shower axis is located at x = 0 cm and y = -35 cm. It is evident that a theoretical response curve for intermediate values of s would fit just as well since the distribution function varies smoothly with s. The level of the tail, indicated at chamber T, seems too high but on the other hand chamber P, which is even closer to the shower axis, showed no signal at all. These numbers, however, are really too small to be statistically reliable. The fitted curve for s = 1.4 seems to be in better qualitative agreement with the data but for this value of s and the corresponding value of N, longitudinal shower theory predicts that the shower was initiated ~ 28 radiation lengths above the observational level and by a primary of energy 5.5×10^{14} ev. Since the thickness of atmosphere above the plane of observation is only about 26 radiation lengths then either the shower, if single-cored, was actually younger or the event was a superposition of two or more showers initiated at lower depths. If this shower were the result of two photon initiated showers arising from a single π^0 decay about 22 radiation lengths above the

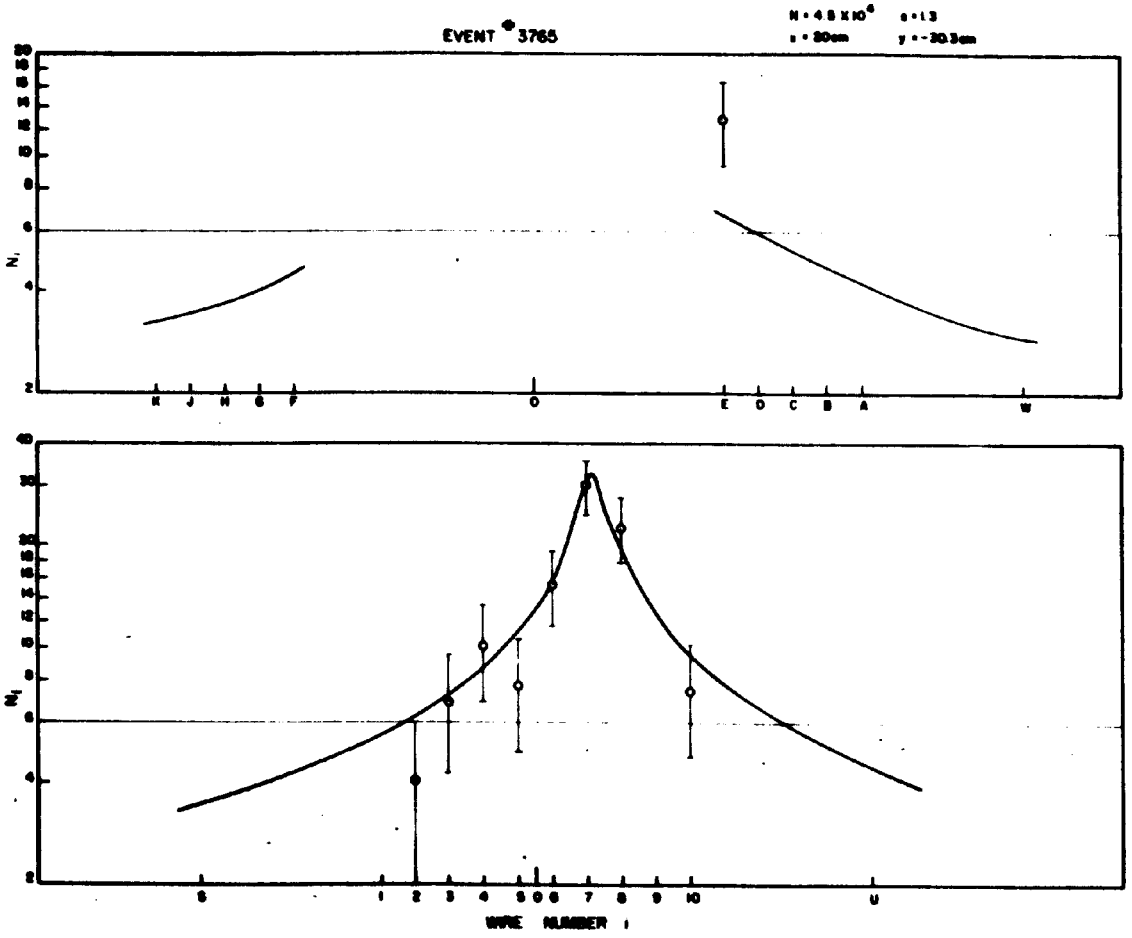

EVENT # 3765
N = 4.8 X 10^6
x = 30cm
y = -30.3cm
N_i
R J H G F
O
E D C B A
W
WIRE NUMBER i
5 1 2 3 4 5 6 7 8 9 10 U

Figure 14.

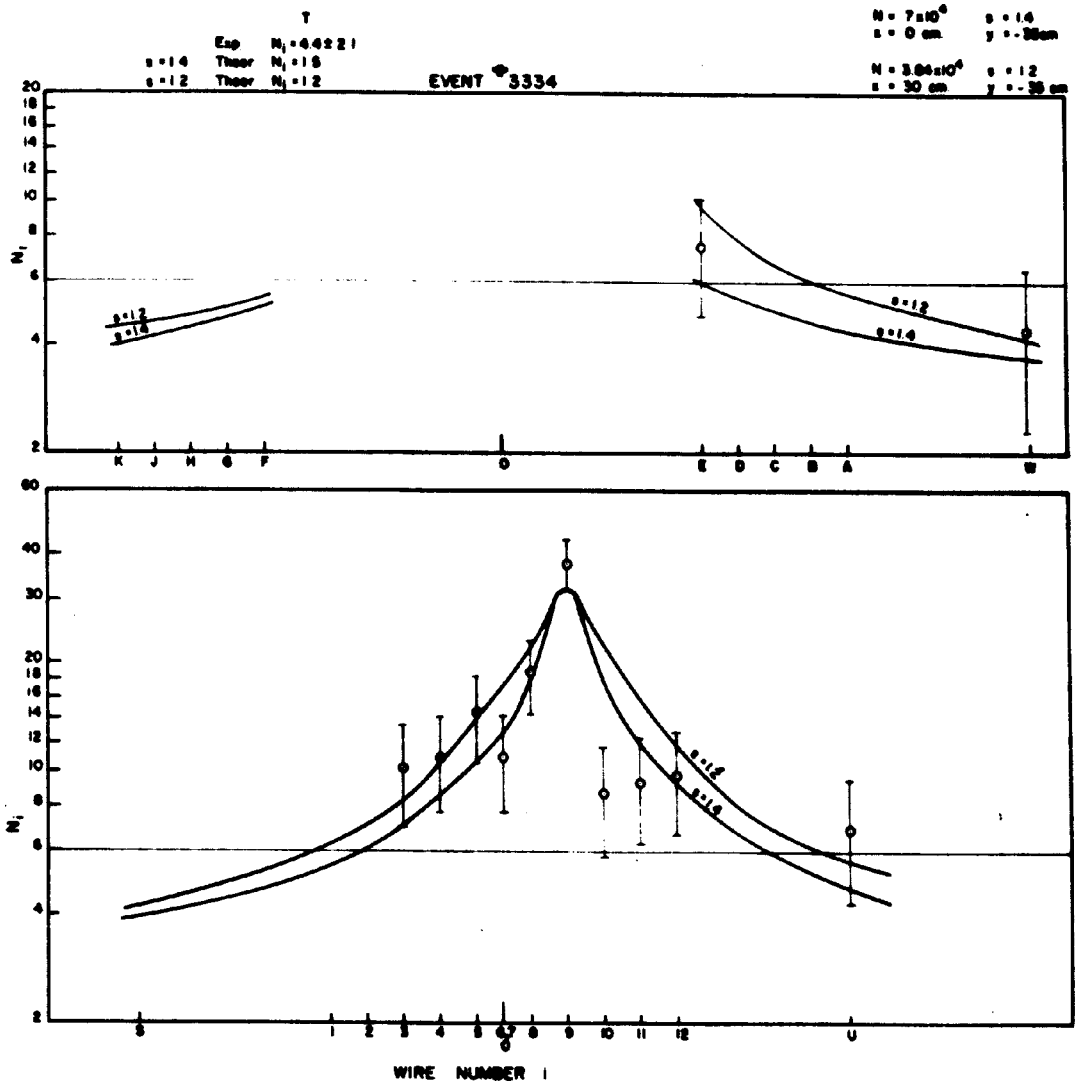

T
Exp N_i = 4.4 ± 2.1
s = 1.4 Theor N_i = 1.8
s = 1.2 Theor N_i = 1.2
EVENT 3334
N = 7×10^6
s = 0 cm
s = 1.4
y = -35cm
N = 3.84×10^6
s = 30 cm
s = 1.2
y = -35 cm
N_i
s = 1.2
s = 1.4
K J H G F
D
E D C B A
W
s = 1.2
s = 1.4
S
1 2 3 4 5 6 7 8 9 10 11 12
U
WIRE NUMBER i

Figure 15.

plane of observation, then the core separation would be less than one centimeter and hence would not be resolved. This prediction is based on a model proposed by Heineman[72]. Both fits are, however, statistically consistent with the data and little more can be said.

In Figure 16 is shown one of two selected events where the shower axis was nearest to one of the side chambers. In this case a fit was attempted by utilizing the side chambers' responses. It is clearly evident from Figure 16 that the proposed fit for $N = 3.63 \times 10^5$ and $s = 1.2$ does not adequately describe this shower. The SW chambers' responses indicate that the density falls off more rapidly than the predicted response. Although no theoretical curves were calculated for showers nearer their maximum than $s = 1.2$, "spot checks" were made at various distances r for $s = 1.0$ and 1.1 while assuming the same location for the shower axis ($x = 150$ cm, $y = -60$ cm). Complete agreement was obtained for the side chambers and SW chambers when $N = 1.2 \times 10^5$ and $s = 1.0$. However, in the main chamber the theoretical response is even lower than for the proposed fit with $s = 1.2$. The scatter of densities in the main chamber, along with the fact that no single theoretical response for single-cored showers gives overall agreement, suggests that some multiple core structure is present. Multiple peaks seem to be present in the main chamber at wires 2, 5, and 8. If this shower were truly at its maximum development, then fluctuations about the average would be a minimum and hence the aforementioned maxima might well be due to young cascades created locally by the N-component. The peaks at wires G and K could also be attributed to locally created showers.

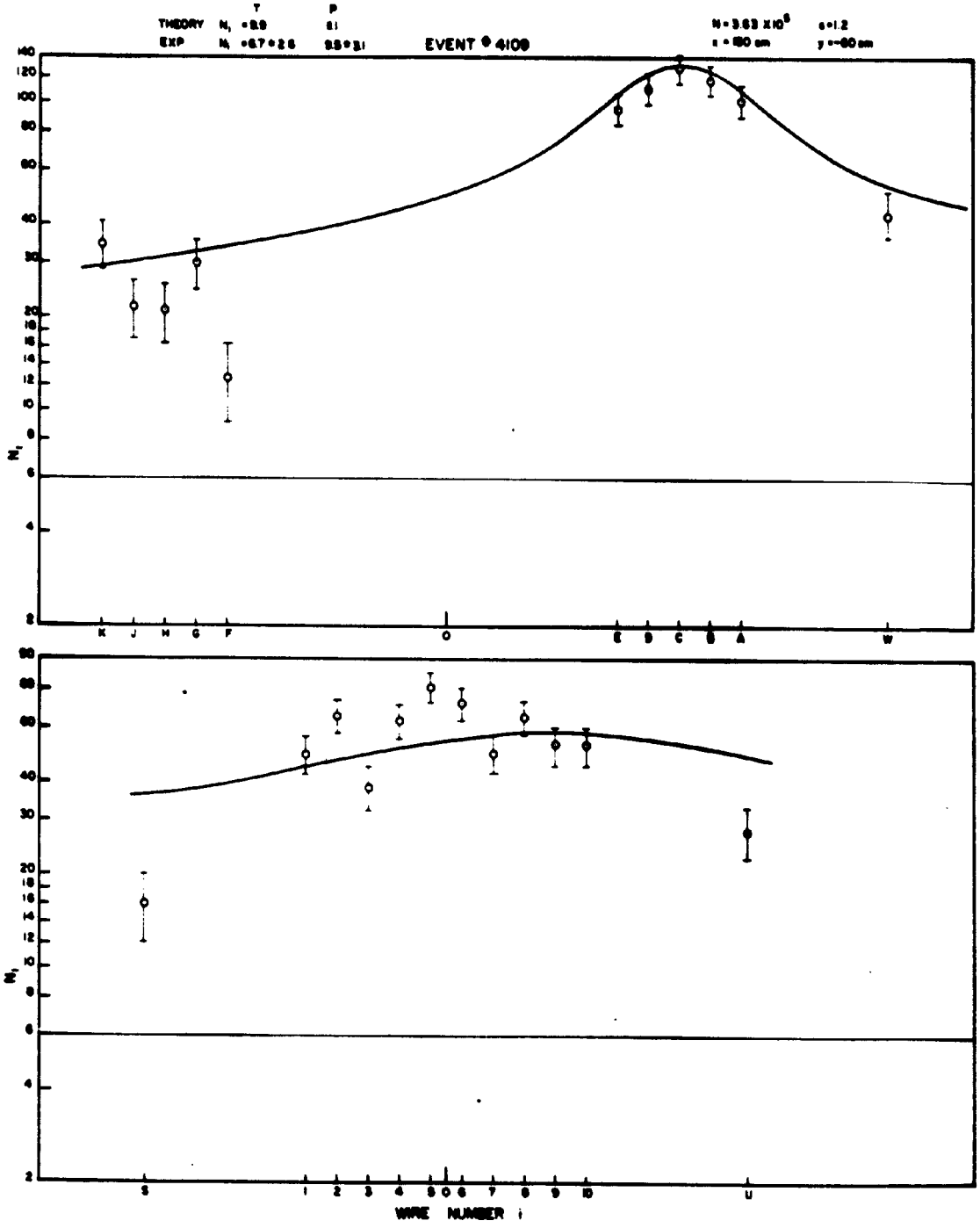

T P
THEORY N, =8.9 21
EXP N, =8.7±2.6 23.5±3.1
EVENT # 4108
N=3.63 X10^6 s=1.2
x=150 cm y=-60 cm
N,
K J H G F O E D C B A W
N,
S 1 2 3 4 5 6 7 8 9 10 U
WIRE NUMBER i

Figure 16.

In event #4089, Figure 17, a main chamber fit was proposed with $N = 8.75 \times 10^4$, $s = 1.2$ and axis located at $x = 30$ cm, $y = -80$ cm. The SW chambers' responses appear to be in good agreement (except for S) but the side chambers again indicate a "background" arising probably from the N-component. Altogether the curve passes through 11 out of 21 flags including the SW chambers.

Events #5148 was very similar to event #4089. Again no single proposed fit agreed, within the limits of the available parameters, with both the main chamber's and the side chambers' responses. The parameters which most nearly agreed with the data were for a shower where $N = 1.82 \times 10^5$, $s = 1.4$ and x and y equalled -30 cm and +20 cm respectively. Unfortunately, the SW chambers were inoperative so that no further information was available. The fact that channels 1, 2, and 3 recorded no electrons is very surprising and it would seem that the apparent asymmetry is perhaps not due to fluctuations in the development of one shower. If one attempts to raise the predicted response of channels K through F while lowering the responses of channels A through E by moving the shower axis further to the left, then the predicted main chamber response is much too flat. The fitted curve predicts that if single-cored, the shower was initiated about 30 radiation lengths above the observational level by a primary particle of energy 2×10^{15} ev. Thus, this fitted curve for a single-cored shower is certainly not correct. Peaks of comparable density are indicated between wires 5 and 6 and at wire H. This is a separation of about 175 cm. It is believed that these are separate cores caused by either multiple π^0-meson production in the original nuclear interaction

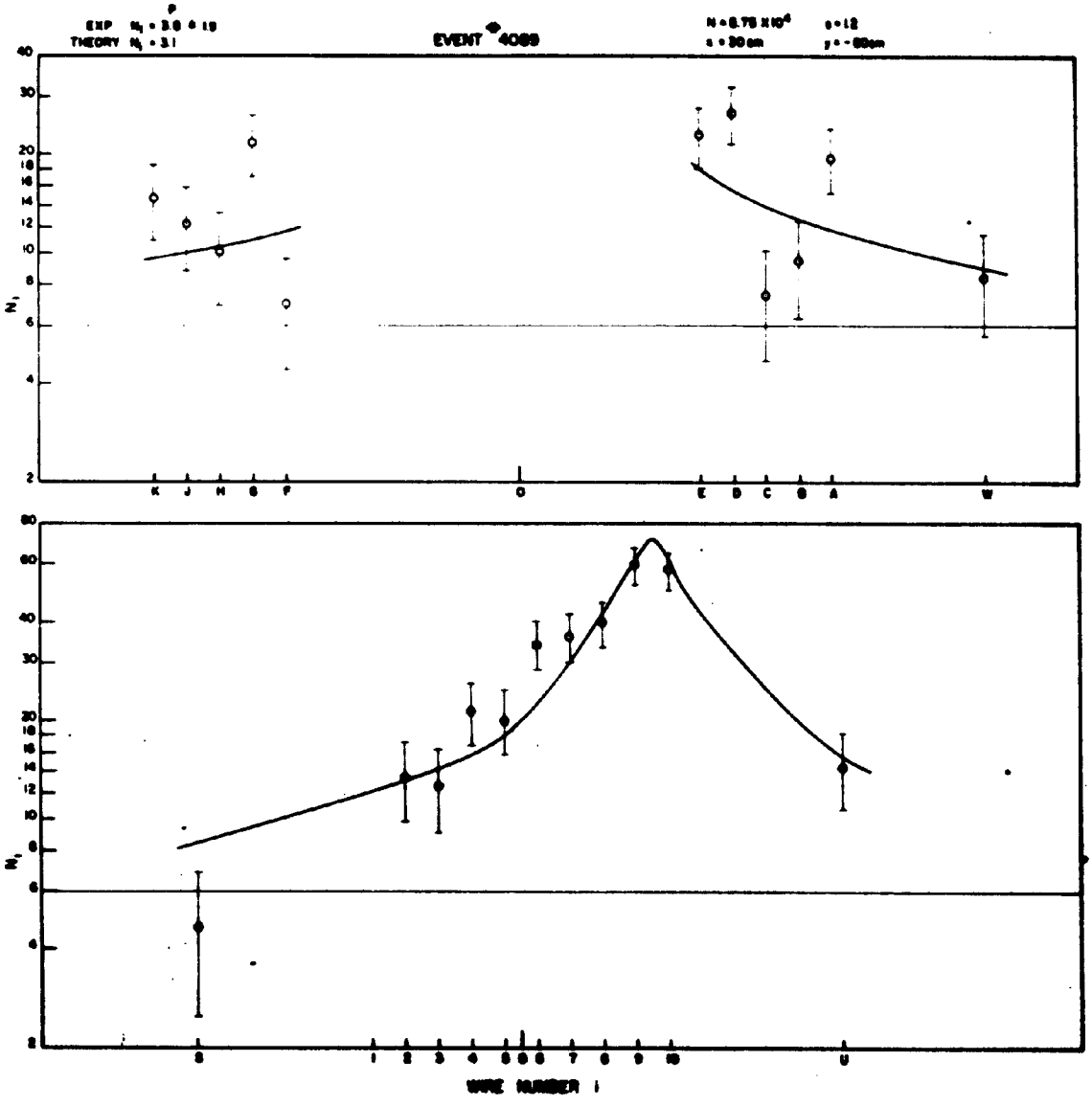


Figure 17.

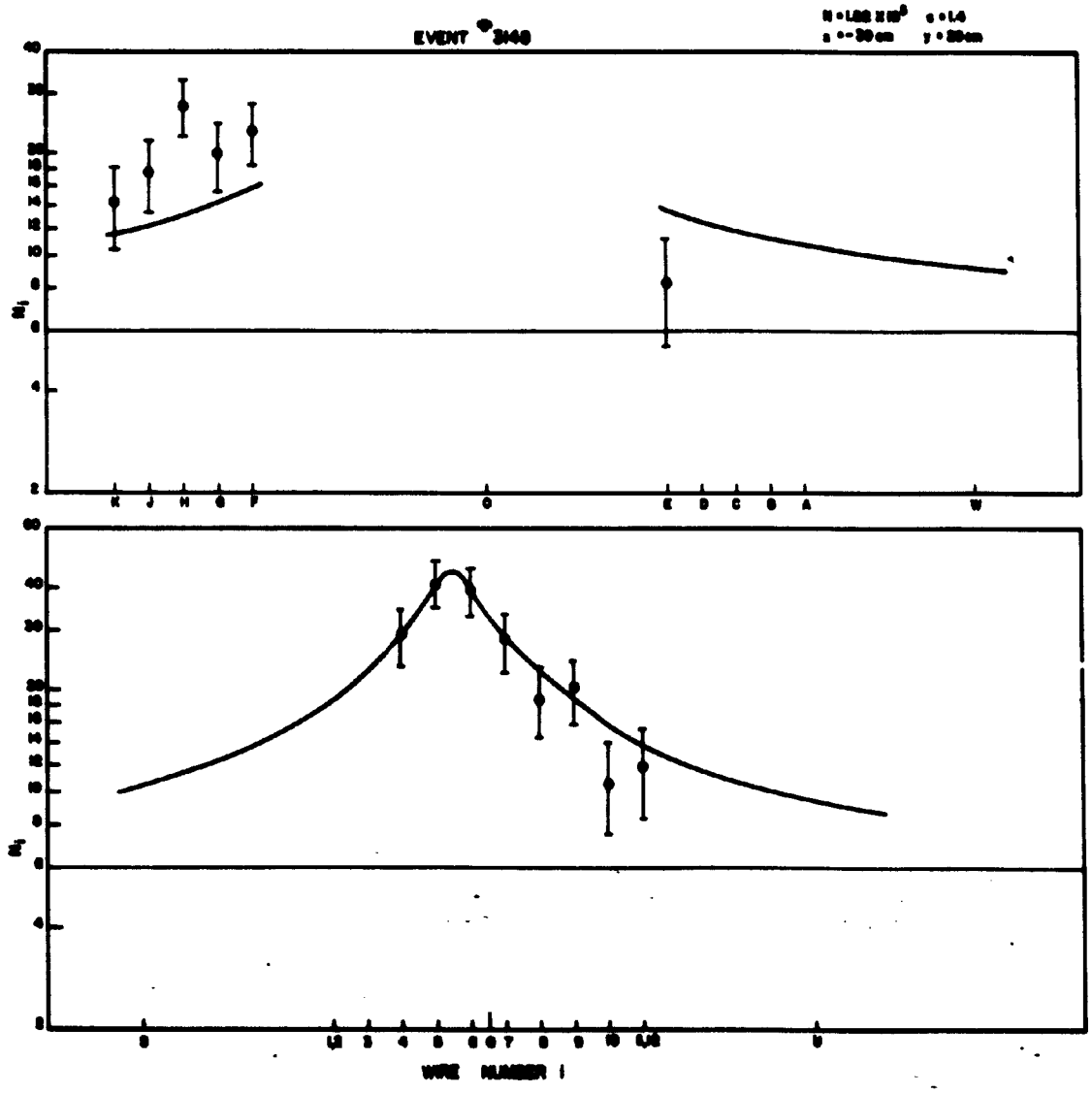


Figure 18.

or by π°-meson production by the N-component cascade. This separation is in agreement with a model proposed by Hazen, Heineman, and Lennox[78]. This model is based on a thermodynamic approximation of Fermi's statistical theory of multiple meson production by single nucleon-nucleon collisions and predicts core separations of from one to ten meters.

Event #4085, shown in Figure 19, is very similar to event #3148 insofar as the fitted response is concerned. Here the shower axis was at x = 30 cm, y = 30 cm. The curve itself is for a shower of 1.95×10^5 particles and an age s = 1.4. Again this fitted response implies single-particle initiation <u>above</u> the atmosphere. No widely separated cores are evident but multiple maxima, attributed to multiple π° production, may be present at wire 2 and possibly 8. Statistically, however, the proposed fit is very good, the curve passing through 16 out of 23 flags. The response of channel 2 is the only one that falls off the curve by more than one standard deviation. Here, a discrepancy of about four standard deviations is noted.

Event #3076, presented in Figure 20, suggests a younger shower than s = 1.2. This event was fitted by a response curve for a shower where $N = 1.15 \times 10^5$ and x = 0 cm, y = -30 cm. However, this proposed fit is <u>not</u> in agreement with the side chambers' data. Channel 12 in the main chamber was not functioning so that significant information may have been lost. No clear evidence of multiple core structure is present although the broad maximum at wires 7 through 10 may be due to unresolved cores. If one attempts to attribute the flat peak to a shower whose axis hit at x = 40 or 50 cm., then the level of the tail

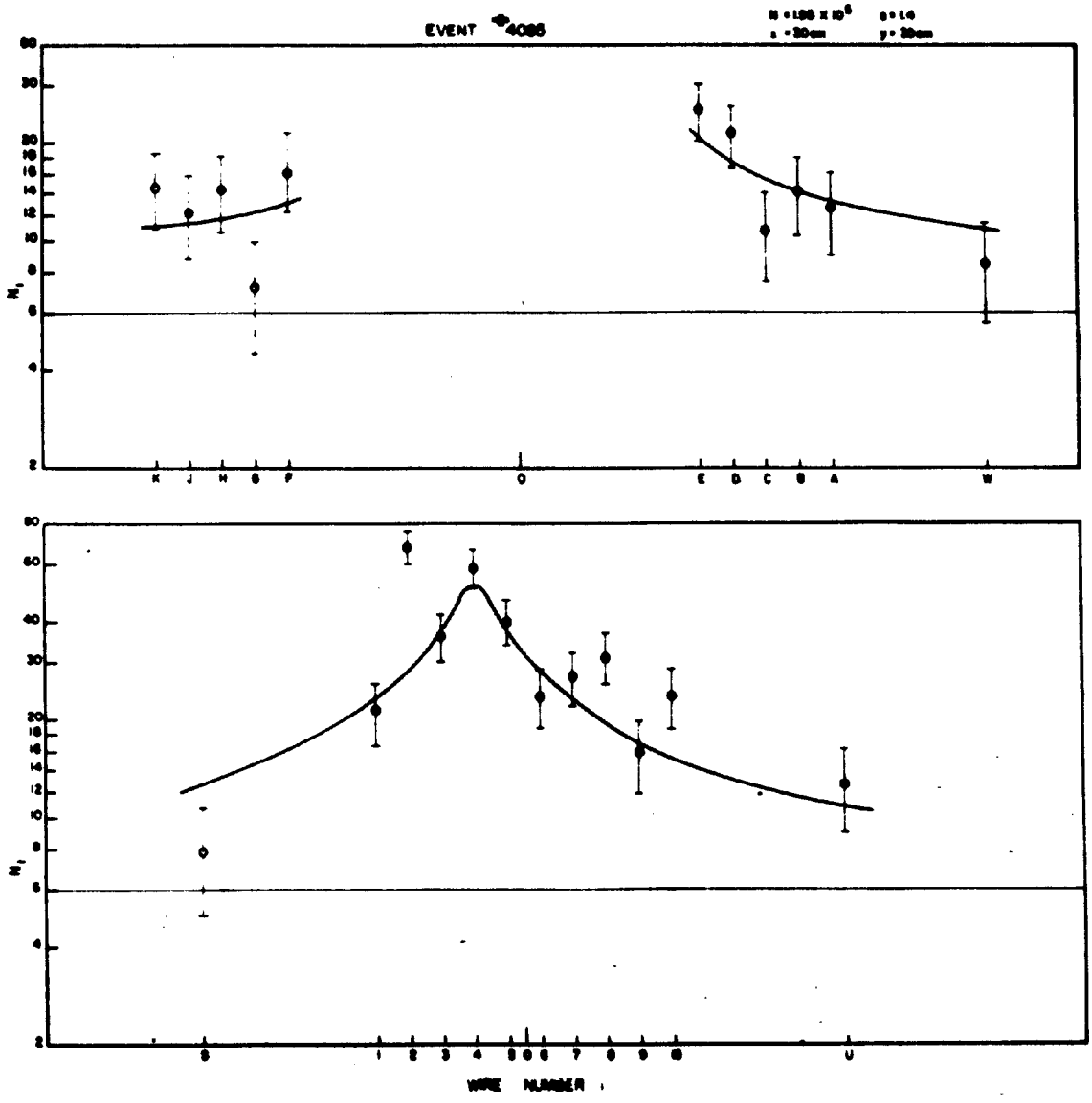


Figure 19.

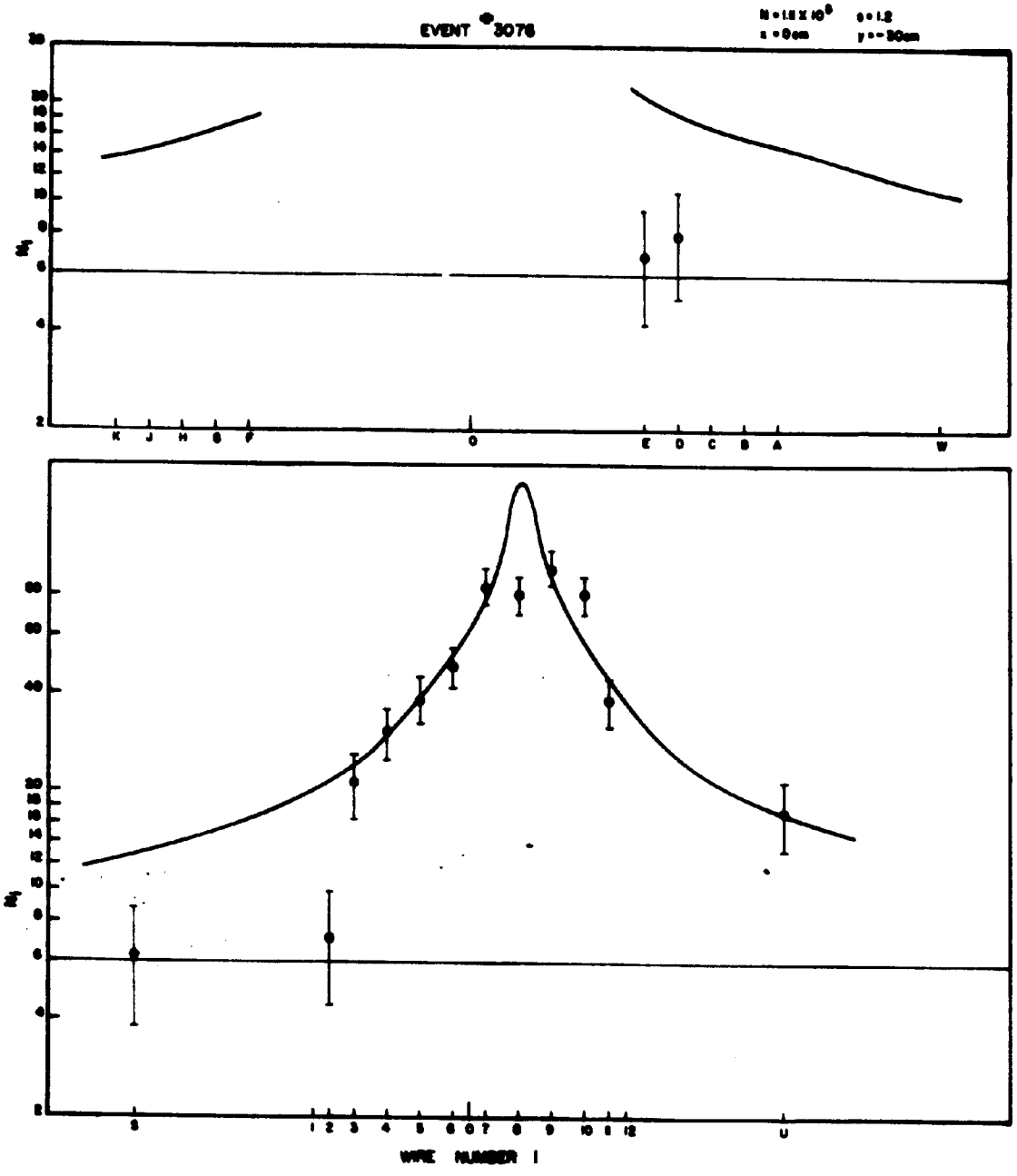

EVENT Φ3076
K J H G F
O
E D C B A
W
S
1 2 3 4 5 6 7 8 9 10 11 12
U
WIRE NUMBER I

Figure 20.

is again too high to be compatible with the side chambers' responses. The above statement is true even for s = 1.0. Thus it would appear that the data presented for this event are explained by assuming a very young shower (s < 1.0) with perhaps a multiplicity of closely spaced cores arising from multiple π^0 production and/or decay-photons from one or more π^0-mesons.

Event #3567 (Figure 21) was analyzed on the basis of a peaked distribution in side chamber channels A through E. The proposed fit is for a shower whose axis hit at x = 185 cm and y = 0 cm. N was 1.24×10^5 and s was chosen to be 1.2. This gave the best possible fit within the limits of the available parameters, although statistically it is not very satisfactory, the curve passing through only 8 of the 15 flags. Channel 12 was inoperative at the time but all others were functioning. The most striking feature of this event is the high density recorded by channels 10 and 11 in the main chamber. The steepness of this distribution (assuming that the response of wires 10 and 11 indicate another core) implies a very young shower (s < 1.0) whose axis has an x-coordinate in the neighborhood of zero. A more probable explanation is that the response of channels 10 and 11 resulted from a heavily ionizing particle released from a star created locally by the N-component.

For the last three events (Figures 22, 23, and 24) no fits were proposed. This was because either no single well-defined maxima were evident or because the showers had ages corresponding to s < 1.2. The latter case is represented in Figure 22. (Note change in scale of ordinate). This was the largest shower for which the data were reduced for analysis

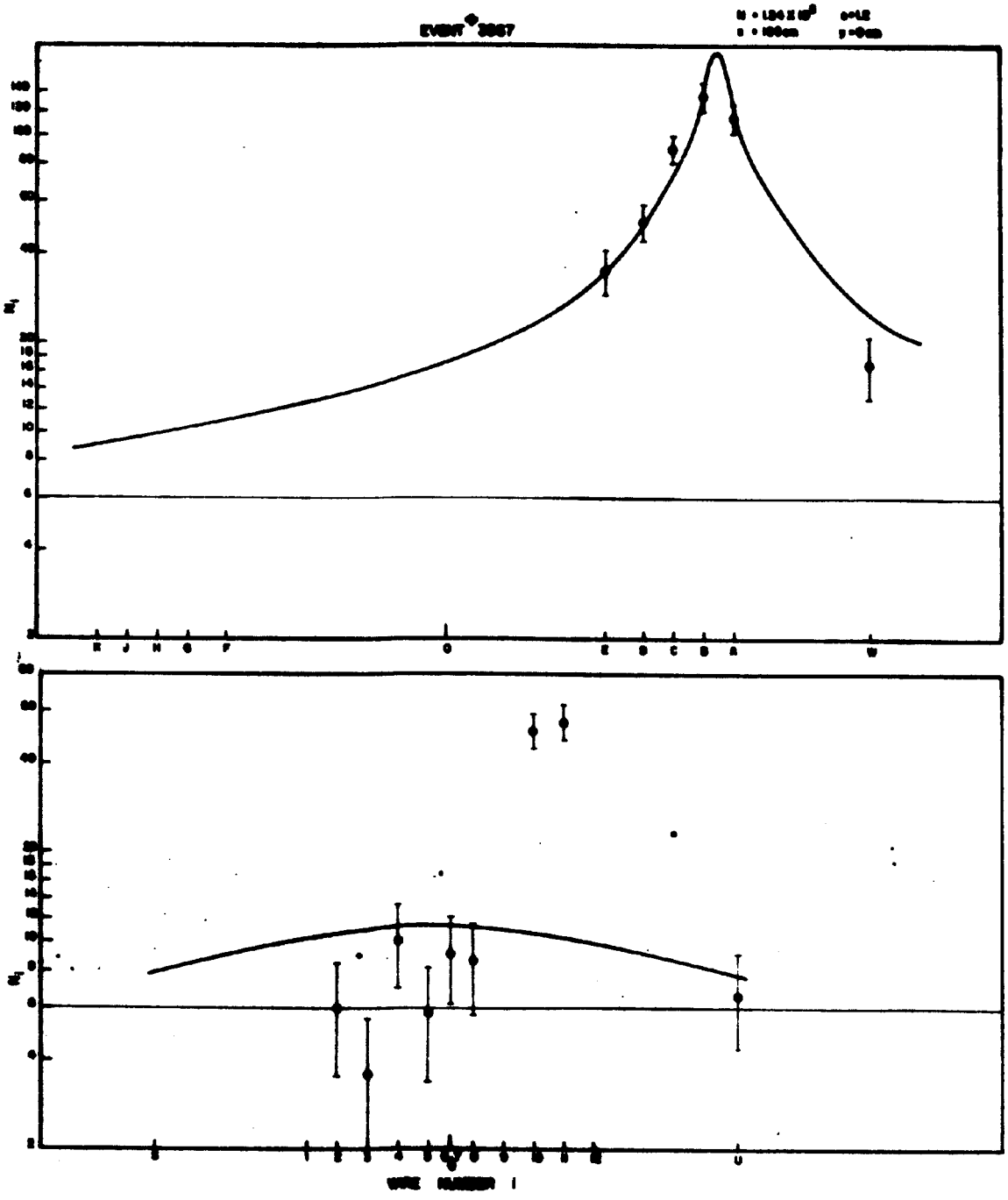


Figure 21.

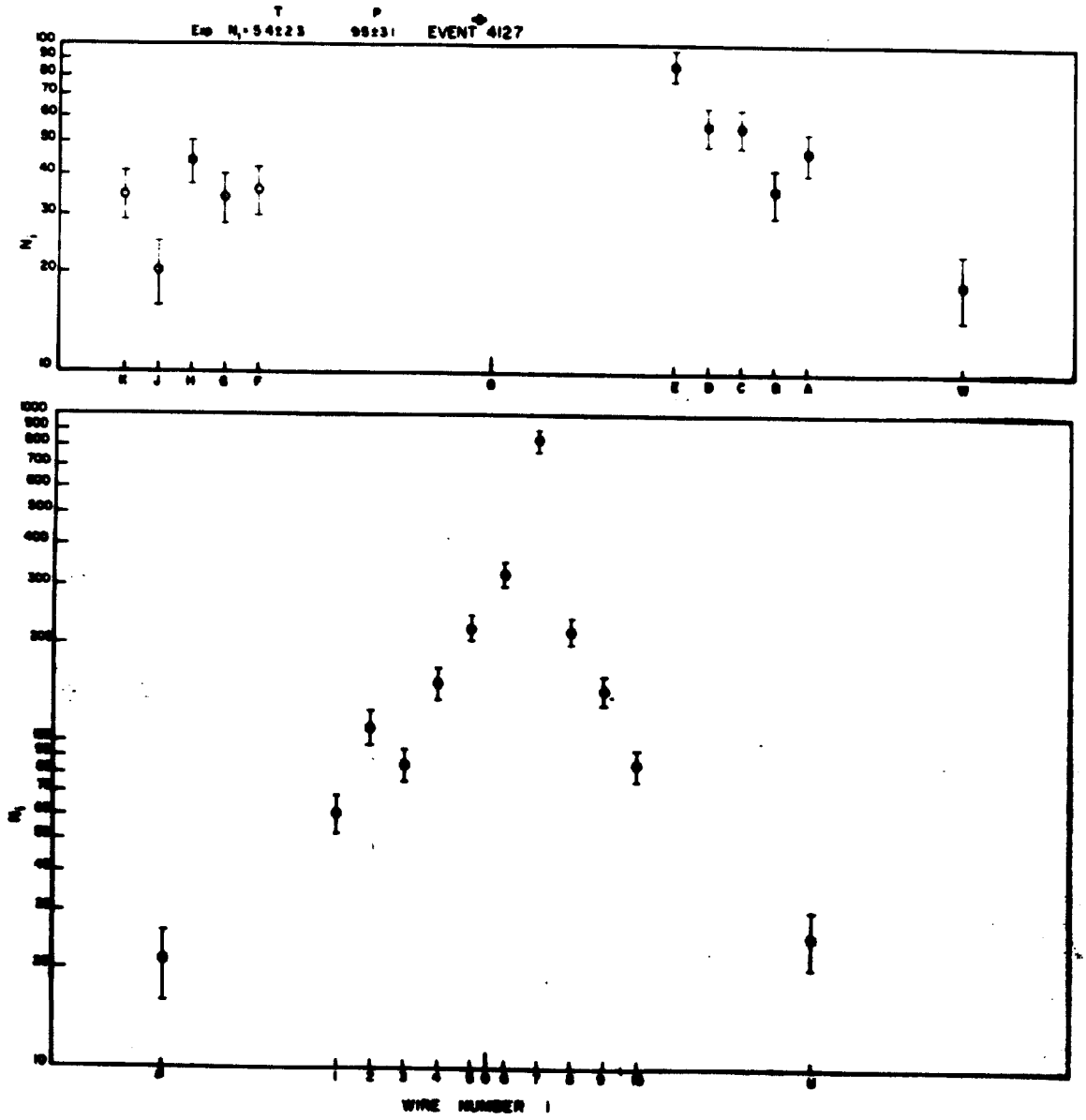


Figure 22.

although larger showers were recorded that did not exhibit a prominent density gradient, i.e. flat showers. This event also displayed one of the most symmetrical lateral distributions (in one dimension) that was encountered. The preamplifier on channel 7 was well above saturation while channels 5, 6, and 8 were just at the overload level. The method of measuring pulse width rather than pulse height (cf. Section 3.4) was used to ascertain the corresponding voltage. It is difficult to estimate the error involved in this measurement but there is reason to believe it to be no larger than about 10%. This shower appears to be at its maximum development. A value for N was estimated by assuming the shower axis to be located at x = 20 cm, y = -20 cm, and with s = 1.0. The level of the tail at chambers T and P resulted in a probable total number of electrons equal to $(1.4 \pm 0.4) \times 10^5$. Auxiliary peaks are noted at wires 2 and E which may be caused by multiple π^0 production.

Event #3426 is presented in Figure 23. Here there was no single well-defined maximum and no satisfactory fit could be achieved for a single-cored shower. The main chamber response seems to indicate several at least partially resolved cores from wires 8 through 12 tending to create a rather broad maximum. The sharp rise from wires 3 to 9 or 10 suggests that the predominant structure is the result of a shower near its maximum. A study of the side chambers' responses clearly indicates the presence of another core near chamber W and having a density comparable to that at wire 10 in the main chamber. The separation between these cores is about 3 meters, a result in agreement with the aforementioned model proposed by Hazen, et al.[78]. These cores are therefore

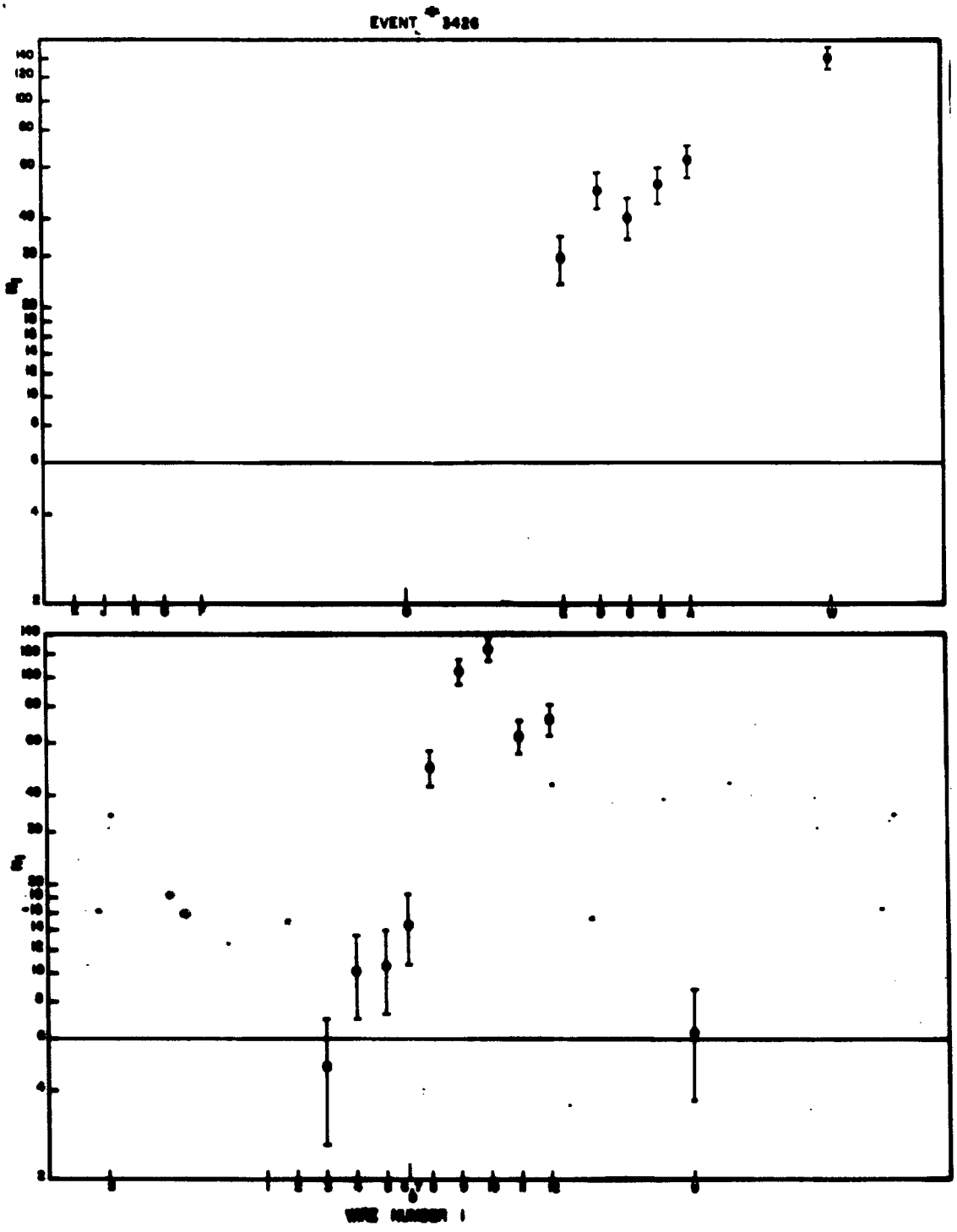


Figure 23.

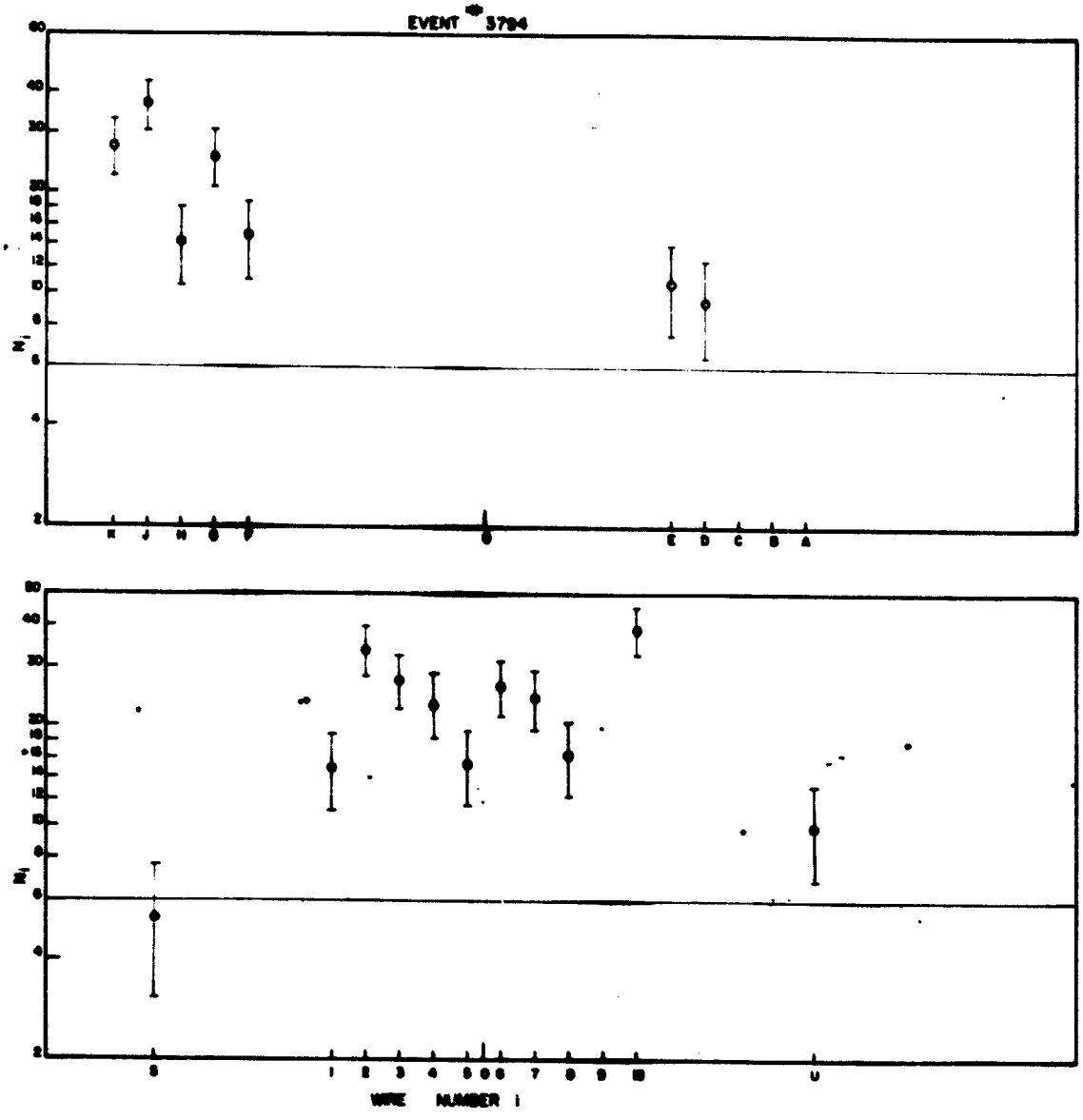


Figure 24.

most probably caused by multiple π°-meson production in the initial nuclear interaction, although multiple π° production by the N-component cascade is not ruled out since the angular divergence of the secondaries (photons) produced at lower depths, and hence with lower energies, would be greater.

The last event to be presented is shown in Figure 24. This event, at first glance, appears to be flat. However, only four out of eighteen channels have responses that lie within $\bar{N}_i \pm \sqrt{\bar{N}_i}$ and no pulses were recorded on chambers T and P. This shower seems to be the result of a superposition of a large number of cores of comparable energies distributed laterally over an area of perhaps 2 or 3 square meters. Again, these multiple cores are believed to originate from multiple π°-meson production in the original nuclear interaction and/or multiple π°-meson production at lower depths by the N-component cascade.

5.5 The Absolute Shower Rate

This experiment also afforded an opportunity to determine the absolute shower rate S(N). The absolute rate or integral number spectrum is defined as the frequency of showers containing a total of N or more electrons and having a central axis that crosses a unit area. Greisen[23] has developed an expression for the number spectrum at sea level as well as another for 3260 meters elevation. His derivation follows from a detailed analysis of measurements of the density spectrum of showers, i.e. the rate at which a detector records a local density of particles exceeding a given value. This method of derivation is justified if the shape of the lateral distribution function does not change with size and

if the number spectrum can be represented by a power law with a slowly varying expcnent. The first condition mentioned above has been found to be satisfied for showers where $N \gtrsim 10^4$ (cf. Reference 57) and the second condition has been experimentally verified for shower sizes up to 10^8 particles(55). Consequently, the rate as indicated by this experiment will be compared with that predicted by Greisen's derived integral number spectrum at sea level. This rate is given by

$$S(N) = (3.5 \pm 0.7) \times 10^{-8} \left(\frac{N}{10^6}\right)^{-[1.55 + 0.0195 \ln \frac{N}{10^6}]} \text{ m}^{-2} \text{ sec}^{-1} \quad (1)$$

In order to effect a comparison between the experimental and predicted rates one must first define an "acceptance area" for showers of various sizes and various ages and then investigate the probability of observing a shower whose axis lies within that area.

The probabilities of triggering for showers where $N = 5 \times 10^4$ and $s = 1.3$ are shown in Figure 25 as estimated contour lines. The "acceptance area" was chosen to be that area bounded by the solid contour. This area is 0.815 m^2. The crosses designate the positions of the shower axes determined in the previous section. Since the lateral distribution is more compressed for younger showers and more spread out for older ones, the triggering efficiency is seen to vary inversely with age. For convenience it will be assumed that the <u>average</u> age of showers at sea level corresponds to $s = 1.3$. This, in fact, is the average age used by Greisen in his derivation of Equation (1). The probability of triggering the geiger tube array then becomes a function only of the relative position of the shower axis with respect to the geiger trays

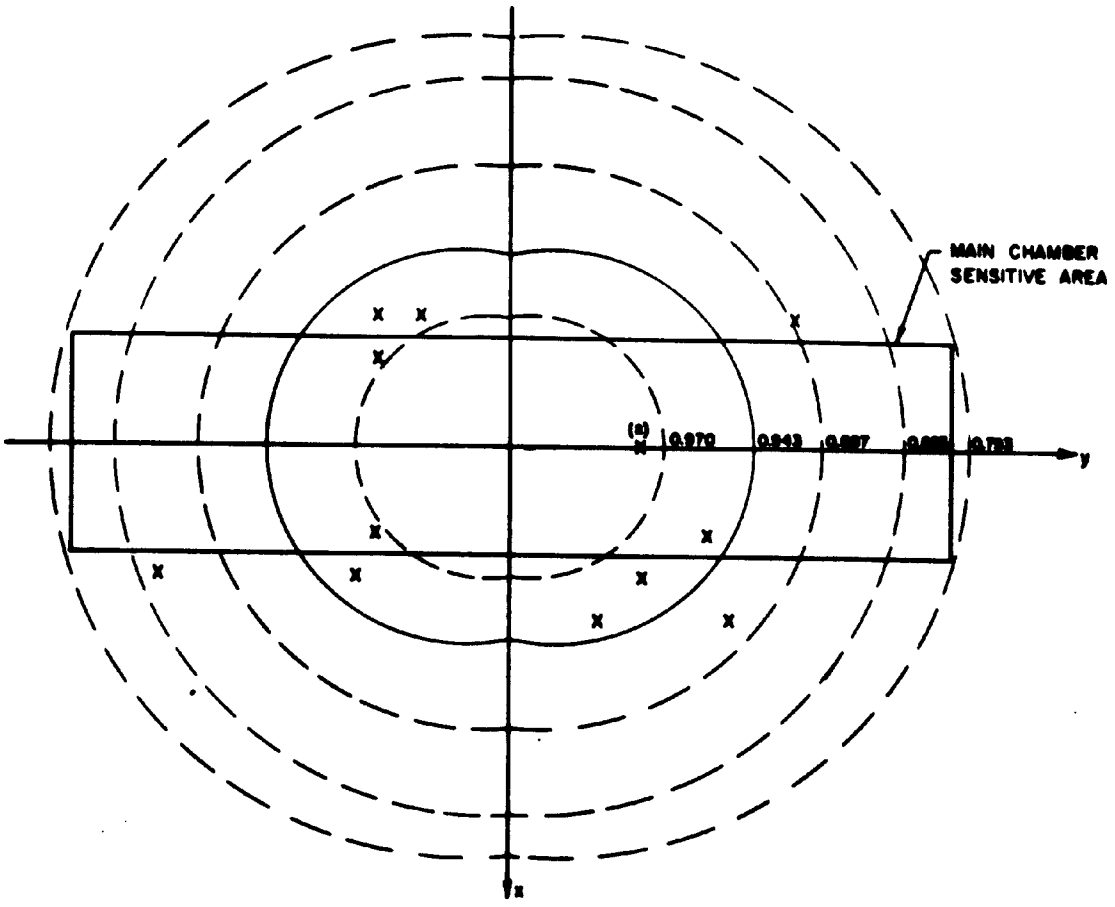


Figure 25. Triggering Probability Loci for $N = 5 \times 10^4$, $s = 1.3$.

and the total number of electrons in the shower. Triggering probabilities for various locations of the shower axis were then calculated for various N, in the range 3×10^4 to 2×10^5, and averaged over the area defined above. The results of these calculations will be designated by P(N), where P(N)dN is then the average probability of observing a shower whose axis lies within the chosen area and which has a total number of electrons between N and N + dN. All the recorded showers having axes within this area had N in the range N_1 to N_2 indicated above so that the predicted absolute shower rate is given by $S = -\int_{N_1}^{N_2} P(N) \frac{dS(N)}{dN} dN$. This integral was first integrated by parts and then evaluated numerically resulting in the following value: $S = (5.11 \pm 1.02) \times 10^{-6}$ showers per square meter per second for $3 \times 10^4 \leq N \leq 2 \times 10^5$. From Figure 25 and/or Section 5.5 it is seen that 10 shower cores were observed within the 0.815 m^2 area and during the total running time of 3.64×10^6 seconds. If one now includes statistical fluctuations in the observed number of showers the experimental number is uncertain by $\pm\sqrt{10}$. Then the experimentally determined rate becomes $(2.97 \pm 0.95) \times 10^{-6}$ m^{-2} sec^{-1}. This is a minimum difference of 4.1% from the predicted rate above at the extreme limits of error.

There are perhaps several reasons that would explain the discrepancy. First, it is possible that some smaller events where $N \sim 3 \times 10^4$ may not have been recognized as having cores near the chambers when scanning the film, and hence would not have been selected for analysis. Second, the older ($s \approx 1.4$) and smaller ($N \approx 3 \times 10^4$) showers, which are expected to have a higher relative frequency, have an average triggering probability

of 0.652. Therefore a significant number of such showers were probably not recorded. Finally, the validity of Equation (1) itself is open to question since it was based on pure electronic cascades and a knowledge of the average age parameter, the latter being only roughly determined from previous experiments. On the whole, when the various sources of uncertainty and rather rough aspects of core location are considered, the measured shower rate seems to be in good agreement with previous observations using geiger counters.

5.6 General Discussion of Results

The purpose of this experiment was to examine the lateral structure of large air showers in the region from the shower axis out to several meters from the axis. This was accomplished by using thin-walled ionization chambers such that the transition effect was negligible. This permitted measurements to be made of the lateral density distribution essentially as it existed in air above the chambers. A comparison of experimental results with the recent theory of Nishimura and Kamata indicated good agreement for small showers ($N < 10^5$) where no multiplicity of cores was observed. A consideration of the shower age could, in most cases, satisfactorily account for any apparent flattening of the lateral distribution near the core.

The events which were studied in detail were selected from all those recorded on the basis of appreciable changes in particle density over the extent of the ionization chamber array ($\sim 2m^2$). The geiger tube triggering arrangement introduced a bias in favor of younger ($s \lesssim 1.3$) showers whose axes passed near the center of the main ionization chamber.

Older showers required $N \gtrsim 10^5$ electrons for comparable triggering efficiency so that the decrease in relative frequency of showers with increasing size resulted in very few old ($s \gtrsim 1.4$) showers being recorded.

The younger ($s \sim 1.0$) and larger ($N > 10^5$) showers showed the most complex structure, suggesting that the N-component cascade accompanying these showers retains, at sea level, a strongly peaked lateral distribution within a few meters of the axis.

One event (#3076) showed evidence of a multiplicity of closely spaced cores arising perhaps from π°-decay-photon showers. Longitudinal shower theory predicts that for core separations of about 40 cm (the resolution of the MW chambers) the energy of the π°-meson, if produced near the top of the atmosphere, would be too small to yield a measurable density of particles at sea level. Furthermore, statistical fluctuations in the number of electrons per wire are probably too large to distinguish with certainty π°-decay cores regardless of resolution.

Two events, #3148 and #3426, exhibited definite evidence of almost equally energetic cores with separations of 1.75 and 3.00 meters respectively. These could only be attributed to a multiplicity of π°-mesons in the initial nuclear interaction or to multiple π°-meson production in later generations of the N-component cascade.

5.7 Summary and Conclusions

In summary, three large thin-walled multi-wire ionization chambers, together with five large thin-walled single-wire chambers, comprising a total of twenty-five and sometimes twenty-seven separate collecting areas, have been used for measuring the ionization produced

by the particles in large air showers near the shower axis. By using a suitable triggering arrangement and high-gain amplifiers it became feasible to observe small showers where the shower rate was about $2\ m^{-2}\ wk^{-1}$. Because of the small transition effect the measured particle density was a good indication of the actual density as it had existed in air. A method of testing for lack of electron attachment was employed to insure the purity of the argon filling agent. Thus, no correction for this effect was necessary. The reduced data then represented the probable number of shower electrons which had passed through each separate collecting area. These experimental results were compared with theoretical predictions based on the Nishimura and Kamata lateral distribution function for single-particle-initiated cascades.

The fluctuations in the lateral spread of a single shower were investigated so as to render a comparison with theory meaningful. It was found that fluctuations for the shower sizes encountered (3×10^4 to 3×10^5 electrons) could be adequately represented by $\sqrt{N_i}$ where N_i is the number of electrons per wire i.

The following conclusions resulted from this comparison of experiment with theory:

1) Over 80% of the showers observed were adequately described by the Nishimura-Kamata lateral distribution function for single-cored showers of the appropriate age s.

2) The soft component of a large air shower is usually the result of either one high energy shower or of lower energy showers with axes separated by less than 40 cm (the resolution of the detectors).

3) Most of the recorded showers, having a total number of electrons between about 3×10^4 and 10^5, could be best described as having an age corresponding to $s = 1.2$. However, a triggering bias was present in favor of younger showers ($s \lesssim 1.3$) for a given total number of electrons.

4) Most of the showers having a total number of electrons greater than 10^5 indicated an anomolous behavior insofar as agreeing with theory for single-cored showers is concerned. These departures from theory were attributed to either multiple π^0-meson production in the original nuclear collision or to π^0-meson contributions arising from later nuclear interactions of the accompanying N-component cascade.

5) Of the showers referred to in 3) above, at least two showed definite evidence of two equally energetic cores with separations on the order of two to three meters. Again, these cores were attributed to multiple π^0-meson production.

6) Two individual shower cores arising from a single π^0-photon-decay could not be resolved with certainty within the resolution of the present equipment, although statistical fluctuations may prevent detecting such cores regardless of resolution.

7) Some showers exhibit an almost flat lateral distribution over a region greater than two meters but less than seven meters. This may be caused by multiple cores of comparable energy.

8) The absolute shower rate, for showers where $3 \times 10^4 \leq N \leq 2 \times 10^5$, is consistent with the number spectrum derived by Greisen on the basis of observations with geiger counters.

APPENDIX A

CALCULATION OF THE CHAMBER POTENTIAL DISTRIBUTION AND "f" -FACTORS

To calculate the "f"-factors referred to in Section 4.1, it is necessary first to know the potential distribution within the chambers. In order to facilitate the calculations both the SW chambers and the MW chambers, as finally connected, may be approximated as infinitely long, grounded, conducting prisms of square cross section. A line charge of strength q per unit length is assumed to lie along the central axis equidistant from the walls. An end view of the SW chambers and a corresponding side view section of the MW chambers is shown in Figure 1. For the SW chambers a = 60 cm and δ, the radius of the wire, = 0.0521 cm. For the MW chambers a = 20 cm and δ = 0.0512 cm

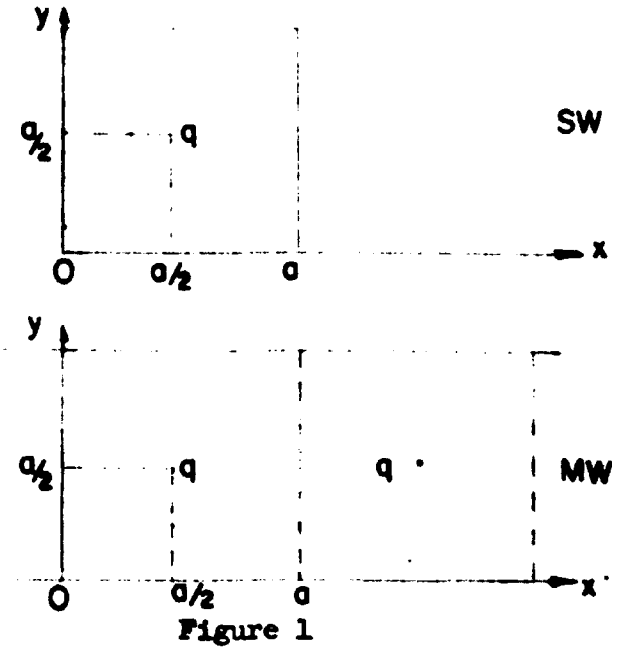


Figure 1

Smythe[77], p 107, problem 51, gives the following analytical expression for the potential distribution for this case:

$$V(x,y) = 4q \sum_{m=1}^{\infty} \frac{\sin \frac{m\pi}{2}}{m \cosh \frac{m\pi}{2}} \sinh \frac{m\pi y}{a} \sin \frac{m\pi x}{a}$$

$$= 4q \sum_{m=1}^{\infty} A(m) \qquad (1)$$

It will be instructive to rewrite Equation (1) in the following way:

$$V(x,y) = 4q \sum_{m=1}^{\infty} \frac{\sin \frac{m\pi}{2}}{m} \left[\tanh \frac{m\pi}{2} \cosh m\pi \left(\frac{1}{2} - \frac{y}{a}\right) - \sinh\left(\frac{1}{2} - \frac{y}{a}\right) \right] \sin \frac{m\pi x}{a} .$$

First, it should be noted that all even terms vanish, and second, that for $m \geq 3$, $\tanh \frac{m\pi}{2} \cong 1.00$. Then,

$$V(x,y) \cong 4q\, A(1) + 4q \sum_{m=3}^{\infty} \frac{\sin \frac{m\pi}{2}}{m} e^{-m\pi\left(\frac{1}{2} - \frac{y}{a}\right)} \sin \frac{m\pi x}{a}$$

$$= 4q\, A(1) + 4q \sum_{m=3}^{\infty} B(m).$$

This may finally be written as:

$$V(x,y) \cong 4q \left[A(1) + \sum_{m=1}^{\infty} B(m) \quad -B(1) \right]$$

$$\text{or } V(x,y) \cong 4q \left[\left(\frac{\sinh \frac{\pi y}{a}}{\cosh \pi/2} - e^{-\pi\left(\frac{1}{2} - \frac{y}{a}\right)} \right) \sin \frac{\pi x}{a} \right.$$

$$\left. + \sum_{m=1}^{\infty} \frac{\sin \frac{m\pi}{2}}{m} e^{-m\pi \left(\frac{1}{2} - \frac{y}{a}\right)} \sin \frac{m\pi x}{a} \right]$$

The first term in the above equation may be simplified and the infinite series in the second term may be written in closed form. This results in the following final expression for the potential distribution:

$$V(x,y) \cong -8q \left[\frac{\cosh \pi\left(\frac{1}{2} - \frac{y}{a}\right)}{e^{\pi} + 1} \sin \frac{\pi x}{a} \right]$$

$$+ q \log \left[\frac{\cosh \pi\left(\frac{1}{2} - \frac{y}{a}\right) + \sin \frac{\pi x}{a}}{\cosh \pi\left(\frac{1}{2} - \frac{y}{a}\right) - \sin \frac{\pi x}{a}} \right] , \qquad (2)$$

where $0 \leq y \leq \frac{a}{2}$ and $0 \leq x \leq a$. Due to symmetry, the potential calculated for any value of y within this interval will be the same as the potential at a - y.

Now, f has been defined in Equation (2) Section 4.1 to be $\frac{\bar{U}_1}{U}$, i.e. the change in potential of the central wire caused by the motion of the electrons alone is this fraction of the change caused by collecting the entire charge, if a uniform distribution of ionization is assumed. As defined above, U is the potential at the walls when the potential at the wire is zero. For the boundary conditions under which Equation (2) was derived, $f = 1 - \frac{\bar{V}}{V_w}$, where V_w is the potential at the surface of the wire when the walls are at zero potential. The implicit assumption has been made that f may be calculated from the original potential field. This is certainly a valid assumption since the voltage pulse induced on the wire is about 10^{-6} times the chamber potential so that the presence of ionization does not appreciably change the electric field.

V_w was chosen as $V(\frac{a}{2} - \delta, \frac{a}{2})$. From Equation (2) this becomes

$$V(\tfrac{a}{2} - \delta, \tfrac{a}{2}) = \delta q \frac{1}{e^{\pi} + 1} \sin \tfrac{\pi}{a} (\tfrac{a}{2} - \delta) + q \log \left[\frac{1 + \sin \frac{\pi}{a} (\frac{a}{2} - \delta)}{1 - \sin \frac{\pi}{a} (\frac{a}{2} - \delta)} \right].$$

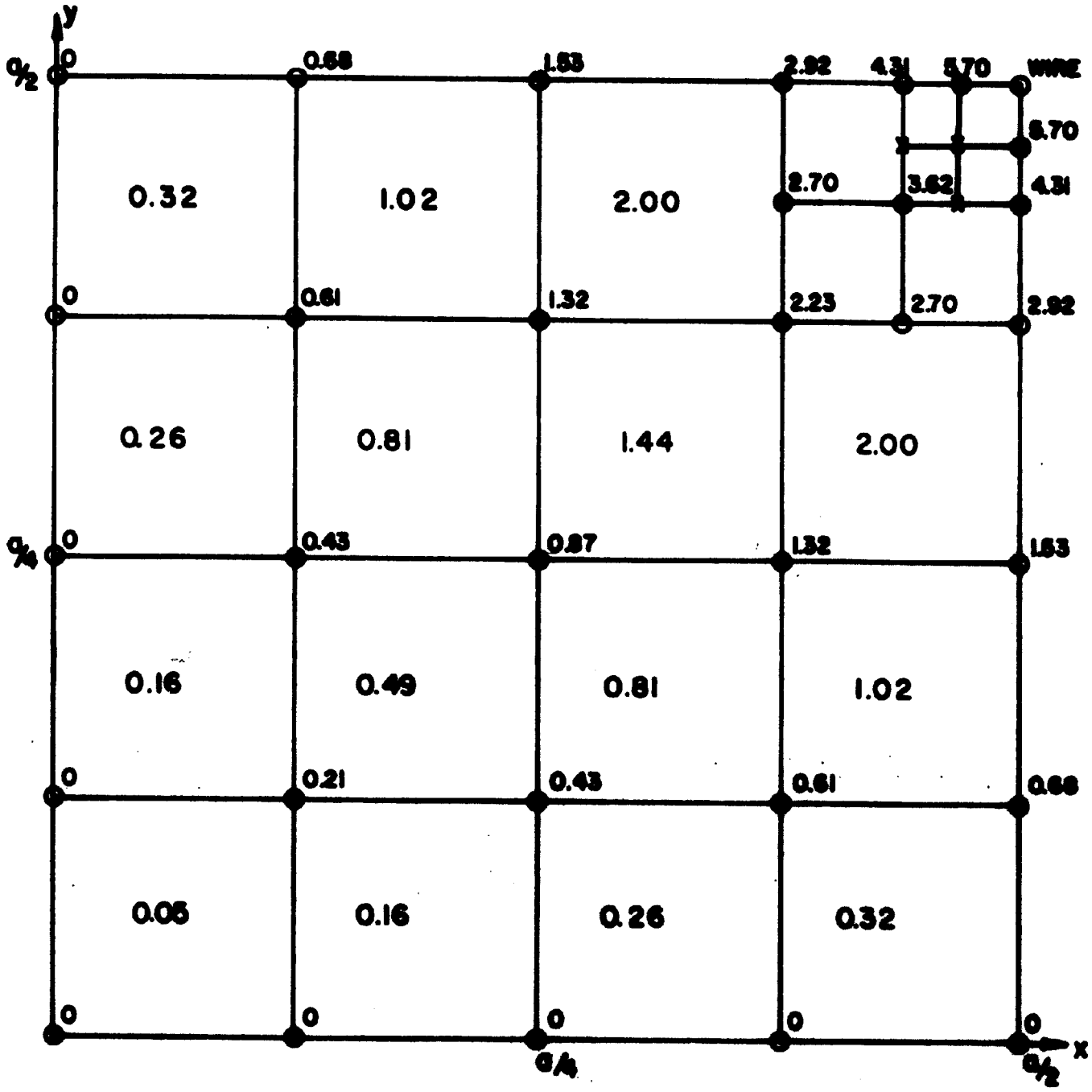
Now, $\sin \frac{\pi}{a} (\frac{a}{2} - \delta) = \cos \frac{\pi\delta}{a}$ and, since $\frac{\delta}{a} \ll 1$, the approximation was made in the first term that $\cos \frac{\pi\delta}{a} \simeq 1$. In the second term $\cos \frac{\pi\delta}{a}$ was expanded to second order so that

$$\frac{1 + \cos \frac{\pi\delta}{a}}{1 - \cos \frac{\pi\delta}{a}} \simeq \frac{2 - \frac{\pi^2\delta^2}{2a^2}}{\frac{\pi^2\delta^2}{2a^2}}.$$ Then, since $\frac{\pi^2\delta^2}{2a^2} \ll 2$, this may be written as $\frac{4a^2}{\pi^2\delta^2}$.

Then, $V(\frac{a}{2} - \delta, \frac{a}{2}) = V_w = -0.33\ q + 2q \log \frac{2a}{\pi\delta}$. This calculation gave values of 11.69 for the MW chambers, and 12.86 for the SW chambers. $\bar{V}$ is of course an integral but, due to the complexity of the potential function, the integration was performed numerically.

In the diagram shown on the following page, the values of $\frac{V(x,y)}{q}$ which were calculated from Equation (2) are shown next to the circled points. Values for $\frac{V}{q}$ at the points marked with crosses were found by cross interpolation of the calculated values. Each number within the squares is the average of the values at the corners. The average value for the upper right hand square was 3.75. Because of the symmetry of the field, only one quadrant was considered.

The average for the sixteen squares was calculated to be 0.929 for both the SW and MW chambers. So $\bar{V} = 0.929\ q$. Thus $f_{MW} = 1 - \frac{0.929}{11.69} = 0.92$, and $f_{SW} = 1 - \frac{0.929}{12.86} = 0.93$. These were the values used in Equation (3), Section 4.2.



Potential Distribution Diagram.

APPENDIX B

CALCULATION OF THE "f" -FACTOR FOR α-PARTICLES IN THE MW CHAMBERS

In Section 4.2 it was stated that the range of Po-α particles in argon at atmospheric pressure is about 5 cm, and that there is an appreciable change in the static MW chamber potential within this distance from the walls.

In Section 4.1 the following general expression for the voltage pulse appearing on the central wire due to the collection of ionization was presented: $V = \frac{e}{CU} \sum_{i=1}^{N_o} U_i$. If U_i does not change appreciably within the α-particle range, then V_α is simply $\frac{e\,N_o}{C}$ where N_o is the total number of ion pairs formed and is equal to $\frac{E_\alpha}{W_o}$.

In the present case, however, a correction must be made and an effective f-factor for α-particles calculated so that

$$V_\alpha = \frac{e\,N_o}{C} f \quad . \qquad (1)$$

It is well known that the specific ionization along the track of an α-particle is not constant. This means that the chamber potential calculated at various points along the α-particle track must be weighted with the number of ion pairs formed in the vicinity of each point. Thus if n_k is the number of ion pairs produced by the α-particle in the kth range interval and $\bar{U}_k$ is the average potential in the kth interval, then $V_\alpha = \frac{e}{CU} \sum_k n_k \bar{U}_k$ where $\sum_k n_k = N_o$.

By comparing this expression with Equation (1) above, an effective f-factor for α-particles may be defined as

$$f_\alpha = \sum_k \frac{n_k}{N_o} \frac{\bar{U}_k}{U} \quad . \qquad (2)$$

It will be assumed here that each α-particle proceeds directly from the source toward the central wire so that the f-factor so calculated will be a minimum value. The summation in Equation (2) should really be an integral, but because the integration is not feasible to perform, finite one-centimeter range intervals were chosen and $\frac{\bar{U}_k}{U}$ was assumed to be equal to the value of $\frac{U_k}{U}$ at the midpoint of each interval.

The specific ionization curve for Po^{210} α-particles in argon at atmospheric pressure was integrated graphically to obtain the fractional number of ion pairs $\frac{n_k}{N_o}$ released in each one-centimeter range interval. For the intervals 0-1 cm, 1-2 cm, and 2-3 cm, the results were 0.244, 0.306, and 0.450, respectively.

Next, the potential V(x,y) was computed from Equation (3) Appendix A for x = 10 cm and y = 0.5, 1.5, and 2.5 cm. This resulted in $\frac{U_{0.5}}{U} = 0.989$, $\frac{U_{1.5}}{U} = 0.965$, and $\frac{U_{2.5}}{U} = 0.944$, for the fractional change in potential at the indicated points. From Equation (2) f_α was calculated to be 0.96. This is a minimum value as mentioned above and if one now considers an isotropic distribution of α-particles from the source a "best" value for f_α may be represented as an average between $f_\alpha = 0.96$ and $f_\alpha = 1.0$, i.e. f_α was chosen to be 0.98. This was the value used in Equation (3) Section 4.2.

BIBLIOGRAPHY

1. B. Rossi, Physik. Z., 33, 304 (1932).
2. B. Rossi, Z. Physik., 82, 151 (1933).
3. P. M. S. Blackett and G. P. S. Occhialini, Proc. Roy, Soc. (London), A139, 699 (1933).
4. P. Auger, R. Maze, and T. Grivet-Meyer, Compt. rend., 206, 1721 (1938).
5. W. Kolhörster, J. Matthes, and E. Weber, Naturwiss. 26, 576 (1938).
6. P. Auger, R. Maze, and J. Robley, Compt. rend., 208, 1641 (1939).
7. G. Cocconi, A. Loverdo, V. Tongiorgi, Phys. Rev., 70, 852 (1946).
8. G. Cocconi, V. Tongiorgi, and K. Greisen, Phys. Rev., 75, 1063 (1949).
9. K. Sitte, Phys. Rev., 87, 351 (1952).
10. G. M. Branch, Phys. Rev., 84, 147 (1951).
11. K. Greisen, W. Walker, and S. Walker, Phys. Rev., 80, 535, 546 (1950).
12. H. Lewis, J. R. Oppenheimer, and S. Wonthuysen, Phys. Rev., 73, 127 (1948).
13. B. Gregory and J. Tinlot, Phys. Rev., 81, 675 (1951).
14. G. Salvini and Y. B. Kim, Phys. Rev., 88, 40 (1952).
15. E. Fermi, Progr. Theoret. Phys., 5, 570 (1950).
16. G. Moliere, Cosmic Radiation, Dover Publications, New York (1946).
17. W. E. Hazen, R. W. Williams, and C. A. Randall, Jr., Phys. Rev., 93, 578 (1954).
18. R. E. Heineman and W. E. Hazen, Phys. Rev., 90, 496 (1953).
19. R. E. Heineman, Phys. Rev., 96, 161 (1954).
20. W. P. Davis, W. E. Hazen, and R. E. Heineman, Nuovo cimento, 12, 255 (1954).
21. B. Rossi and K. Greisen, Rev. mod. Phys., 13, 240 (1941).

22. B. Rossi, High Energy Particles, Prentice-Hall, New York (1952).

23. K. Greisen, Progress in Cosmic Ray Physics, Vol. III, Chapter I, Interscience Publishers, Inc. New York (1956).

24. H. Euler and H. Wergeland, Astrophys. Norveg., 3, 165 (1940).

25. L. Landau, J. Phys. U.S.S.R., 3, 237 (1940).

26. S. Z. Belenky, J. Phys. U.S.S.R., 8, 9 (1944).

27. G. Moliere, Naturwiss., 30, 87 (1942).

28. G. Moliere, Vorträge über Kosmische Strahlung, (ed. W. Heisenberg; Springer, Berlin) p. 446 (1953).

29. J. Roberg and L. W. Nordheim, Phys. Rev., 75, 444 (1949).

30. G. Poiani and C. Villi, Nuovo cimento, 9, 1109 (1952).

31. A. Borsellino, Nuovo cimento, 7, 523, 638, and 700 (1950).

32. L. Janossy, Cosmic Rays, Oxford Univ. Press, London (1948).

33. L. Janossy, Proc. Phys. Soc., (London), A63, 1009 (1950).

34. J. Nishimura and K. Kamata, Progr. Theoret. Phys., 5, 899 (1950).

35. J. Nishimura and K. Kamata, Progr. Theoret. Phys., 6, 628 (1951).

36. J. Nishimura and K. Kamata, Progr. Theoret. Phys., 7, 185 (1952).

37. G. T. Zatsepin, I. L. Rosental, L. I. Saritcheva, G. B. Khristiansen and L. K. Eidus, Izv. Akad. Nauk. SSSR, Ser. Fiz., 17, 39 (1953).

38. L. Eyges and S. Fernbach, Phys. Rev., 82, 23 and 287 (1951).

39. S. Fernbach, Phys. Rev., 82, 288 (1951).

40. H. S. Green and H. Messel, Phys. Rev., 88, 331 (1952).

41. G. Poiani and C. Villi, Nuovo cimento, 9, 825 (1952).

42. N. Arley, Proc. Roy. Soc. (London), A168, 519 (1938).

43. G. Cocconi, V. C. Tongiorgi and K. Greisen, Phys. Rev., 76, 1020 (1949).

44. G. Fujioka, Internat. Conf. Theor. Phys. (Japan) (1953).

45. S. R. Haddara and D. Jakeman, Proc. Phys. Soc. (London), A66, 549 (1953).

46. P. H. Barrett, L. M. Bollinger, G. Cocconi, Y. Eisenberg and K. Greisen, Rev. mod. Phys., 24, 133 (1952).

47. W. E. Hazen, Phys. Rev., 85, 455 (1952).

48. J. Ise, Jr. and W. Fretter, Phys. Rev., 76, 933, (1949).

49. J. M. Blatt, Phys. Rev., 75, 1584 (1949).

50. K. E. Relf, Phys. Rev., 97, 172 (1955).

51. R. W. Williams, Phys. Rev., 74, 1689 (1948).

52. I. D. Campbell and J. R. Prescott, Proc. Phys. Soc. (London), A65, 258 (1952).

53. H. L. Kasnitz and K. Sitte, Phys. Rev., 94, 977 (1954).

54. K. Sitte, D. L. Stierwalt and I. L. Kofsky, Phys. Rev., 94, 988 (1954).

55. G. Clark, J. Earl, W. Kraushaar, J. Linsley, B. Rossi, and F. Scherb, Nature, 180, 353-356, 406-409, (1957).

56. T. E. Cranshaw, W. Galbraith, and N. A. Porter, Phil. Mag. (Eighth Ser.) Vol. 2, 891 (1957).

57. E. W. Kellermann, T. Shaw, and G. O. Walker, Proc. Phys. Soc. (London), 71, Pt. 3, 491 (1958).

58. O. El-Mofty, Phys. Rev., 92, 461 (1953).

59. W. E. Hazen, Nuovo cimento, 11, 393 (1954).

60. E. Fermi, Progr. Theoret. Phys., 5, 570 (1951). and Phys. Rev., 81, 683 (1951).

61. W. Heisenberg, Vortrage über Kosmische Strahlung, (Springer, Berlin) p. 148 (1953).

62. L. Landau, Izv. Akad, Nauk S.S.S.R., Ser. Fiz., 17, n. 1. (1953).

63. W. L. Kraushaar and L. J. Marks, Phys. Rev., 93, 326 (1954).

64. M. F. Kaplon, B. Peters, and H. L. Bradt, Phys. Rev., 76, 1735 (1949).

65. J. J. Lord, J. Fainberg and M. Schein, Phys. Rev., 80, 970 (1950).

66. E. Pickup and L. Voyvodic, Phys. Rev., 84, 1190 (1951).

67. D. Lal, Y. Pal, B. Peters and M. S. Swami, Proc. Ind. Acad. Sci., A36, 75 (1952).

68. M. F. Kaplon and D. M. Ritson, Phys. Rev., 85, 932 (1952) and Phys. Rev., 88, 386 (1952).

69. R. A. Marshak, Meson Physics, McGraw-Hill, New York (1952).

70. G. Cocconi, Phys. Rev., 93, 1107 (1954).

71. B. Rossi and H. Staub, Ionization Chambers and Counters, McGraw-Hill, New York (1949).

72. R. E. Heineman, Thesis, University of Michigan (1952),(Unpublished).

73. W. Jesse, H. Forstat, and J. Sodanskis, Phys. Rev., 77, 782 (1950).

74. F. E. Driggers, Phys. Rev., 87, 1080 (1952).

75. W. P. Davis, Thesis, University of Michigan (1954),(Unpublished).

76. F. E. Driggers, Thesis, University of Michigan (1951),(Unpublished).

77. W. R. Smythe, Static and Dynamic Electricity, McGraw-Hill, New York (1939).

78. W. E. Hazen, R. E. Heineman, and E. Lennox, Phys. Rev. 86, 198 (1952)